The lowest triplet state of 1,3,5-hexatrienes: Quantum chemical force field calculations and experimental resonance Raman spectra

ARTICLE *in* THE JOURNAL OF CHEMICAL PHYSICS · JUNE 1989

Impact Factor: 2.95 · DOI: 10.1063/1.456361

The lowest triplet state of 1,3,5-hexatrienes: Quantum chemical force field calculations and experimental resonance Raman spectra

Fabrizia Negri and Giorgio Orlandi
Dipartimento di Chimica "G.Ciamician", University of Bologna, I-40126 Bologna, Italy

Albert M. Brouwer
Laboratory of Organic Chemistry, University of Amsterdam, Nieuwe Achtergracht 129, NL-1018 WS Amsterdam, The Netherlands

Frans W. Langkilde and Robert Wilbrandt
Department of Chemistry, Risø National Laboratory, DK-4000 Roskilde, Denmark

(Received 23 November 1988; accepted 24 January 1989)

Theoretical and Raman spectroscopic studies are presented of *E* and *Z*-1,3,5-hexatriene and their 3,4- and 2,5-dideuteriated analogs in ground and excited triplet states. The T_1 potential energy surface is calculated from extended SCF-LCAO-MO-CI theory. Energy minima and equilibrium geometries are determined in T_1. Frequencies and normal modes of vibration are calculated for the minima of the T_1 and S_0 states. Energies of higher triplet levels are computed and oscillator strengths for the transitions from T_1 to T_n are determined. The displacements in equilibrium geometries between the T_1 and the T_n level corresponding to the strongest $T_1 \rightarrow T_n$ transitions are calculated and are used to estimate the intensities of the resonance Raman spectra of the T_1 state under the assumption of a predominant Franck–Condon scattering mechanism. The results indicate that the planar *E* and *Z* forms of hexatriene and its analogs are the only ones contributing substantially to the $T_1 \rightarrow T_n$ absorption and the T_1 resonance Raman spectra found in the present experiments. The existence of a twisted form in the T_1 state cannot be ruled out, but its contribution to the resonance Raman spectra corresponding to an electronic $T_1 \rightarrow T_n$ transition around 315 nm is likely to be much weaker than that of the *E* or *Z* forms. Satisfactory agreement is found between the calculated and experimentally determined resonance Raman spectra. An assignment is obtained for the experimentally determined vibrational modes in T_1. The theoretical results indicate a substantial rotation of normal modes from S_0 to T_1.

I. INTRODUCTION

The electronic structure and spectroscopy of short polyenes has been studied widely during the past decade.[1] Most work has dealt with ground state and excited singlet state properties. These have been summarized recently by Hemley *et al.*[2] Less attention has been devoted to the triplet manifold.

A number of theoretical calculations of 1,3,5-hexatriene have appeared in the literature. These include both *ab initio*[3–12] and semiempirical[2,12–14] methods.

The geometry of *E*- and *Z*-hexatriene in the ground state in the gas phase has been determined by electron diffraction.[15,16] Vibrational spectroscopy has been used by a number of authors as a means to investigate the ground state of hexatriene.[17–25] These studies include Raman and infrared spectra of hexatriene-d_0[17–25] and tetradeuteriated[19–23] hexatrienes. Furthermore, vibrational spectra of less stable conformers have been reported.[26,27]

The triplet states of 1,3,5-hexatriene (HT) and methylated derivatives have been studied by direct singlet–triplet absorption spectroscopy,[28,29] electron energy loss spectroscopy,[30] time-resolved absorption spectroscopy,[31,32] and time-resolved resonance Raman spectroscopy.[32–35] The vertical energies of the lowest triplet state T_1 of *E*-1,3,5-hexatriene (EHT) and *Z*-1,3,5-hexatriene (ZHT) determined by electron energy loss spectroscopy are 2.03 and 2.07 eV, respectively. A first maximum for the $T_1 \rightarrow T_n$ absorption spectrum of 1,3,5-heptatriene was found around 315 nm with a first-order decay rate of $k = 3.4 \times 10^6$ s^{-1}.[32] Similar first-order decay rates were found for EHT and ZHT from resonance Raman experiments.[35] The resonance Raman spectra of triplet EHT and ZHT were reported to be identical indicating equilibration with respect to twisting around the central C=C double bond in the T_1 state during the lifetime of the triplet state. In contrast the resonance Raman spectra of triplet *E*- and *Z*-2,5-dimethyl-1,3,5-hexatriene were reported to be different from each other, which was interpreted in terms of nonequilibration of excited rotamers (NEER) in the triplet state.[34] No detailed assignment of the triplet state resonance Raman spectra was given.

In order to give a more detailed assignment of the triplet vibrations we report in the present paper Raman spectra from the ground state of *E*-3,4-d_2-1,3,5-hexatriene (*E*-3,4-d_2-HT) and *E*-2,5-d_2-1,3,5-hexatriene (*E*-2,5-d_2-HT) as well as time-resolved resonance Raman spectra of these two compounds in their lowest excited triplet T_1 state. Furthermore, quantum chemical force field (QCFF/PI) and CNDO/S calculations are performed on the ground and excited triplet states of the *E* and *Z* isomers of HT, 3,4-d_2-HT and 2,5-d_2-HT. The previously reported triplet state resonance Raman spectra of EHT and ZHT[35] and the new experimental results presented here are then discussed in the light of the theoretical calculations.

 0021-9606/89/115944-20$02.10

II. EXPERIMENTAL METHODS

A. Materials

Acetonitrile-d_0 (Merck, LiChrosolv), acetonitrile-d_3 (Fluka, puriss., >99.8% D), and acetone (Ferak, p.a.) were used as received. The deuteriated 1,3,5-hexatrienes were prepared from the corresponding deuteriated 3-hexene-2,5-diols via pyrolysis of their acetates at 530 °C/0.1 mm, followed by separation of the reaction mixture using preparative gas chromatography (GC) (squalane column). 2,5-Dideuterio-3-hexene-2,5-diol was obtained by reduction of 3-hexene-2,5-dione[36] with $LiAlD_4$ (>98% D). Reduction of 3-hexyne-2,5-diol (Aldrich) with $LiAlD_4$ followed by quenching with D_2O[37] afforded 3,4-dideuterio-3-hexene-2,5-diol. The diols were converted to the acetates by treatment with acetic anhydride and pyridine. ^1H NMR spectrometry (Bruker WM300, 300 MHz) of the deuteriated products indicated a high deuterium content (>95%). No isomeric or other impurities were found by capillary GC on the samples. The deuterium incorporation was judged to be high, since in the Raman spectra no bands were found that were attributable to species other than *E*-3,4-d_2-HT and *E*-2,5-d_2-HT. The purified samples were put in glass capillaries under nitrogen, and the capillaries were cooled briefly and sealed. Throughout the transient experiments the capillaries with trienes were opened and solutions prepared and transferred to sample cells under an Ar atmosphere. Prior to the addition of triene the solvents were purged with Ar for more than 35 min.

B. Methods

The details of experimental procedures for recording conventional Raman spectra[25] and for time-resolved experiments[34] have been described previously. Briefly, the triplet state of the triene was produced by exciting acetone as sensitizer with a pump pulse from an excimer laser at 308 nm. The resonance Raman spectrum of hexatriene in its T_1 state was obtained by using the second harmonic at 317.5 nm from a Nd:YAG-pumped dye laser as probe pulse. The triplet state spectra were then obtained by subtraction procedures. The isomeric purity of the samples before and after the experiments was monitored by means of GC and by evaluating the preresonance Raman spectra of the solutions with respect to vibrational bands from the ground states of different hexatriene isomers.

III. EXPERIMENTAL RESULTS

A. Ground state

The Raman spectrum of neat *E*-3,4-d_2-1,3,5-hexatriene excited at 514.5 nm is shown in Fig. 1 and the resulting wave numbers and polarizations are tabulated in Table I. Figure 2(a) shows the ground state Raman spectrum of an Ar-saturated solution of ≈9 mM *E*-3,4-d_2-HT in acetonitrile-d_3 with pulsed excitation at 317.5 nm after subtraction of solvent. Figure 2(b) shows the difference spectrum obtained by subtraction of a spectrum of a solution before the transient experiments from that obtained of the same solution after irradiation with 2000 pump-and-probe pulses. Hence spectrum 2(B) is indicative[35] of the isomerization from the *E* to the *Z* isomer of 3,4-d_2-HT, the negative bands being interpreted as a decrease in concentration of the *E* and the positive bands as an increase in concentration of the *Z* isomer. The solution used to obtain spectrum 2(B) was an Ar-saturated solution of 0.54 M acetone and ≈9 mM *E*-3,4-d_2-HT in acetonitrile-d_3. GC analysis showed no isomeric impuri-

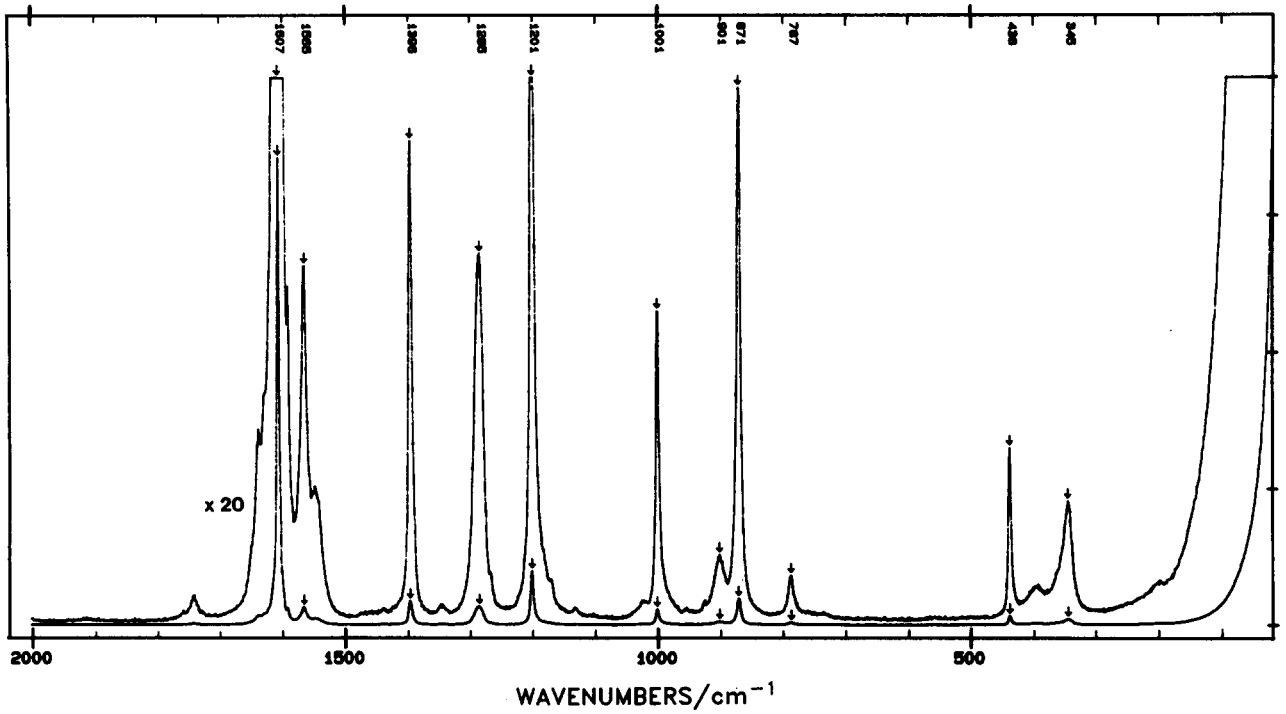

FIG. 1. Raman spectrum of neat *E*-3,4-d_2-1,3,5-hexatriene excited at 514.5 nm.

TABLE I. Wave numbers (cm^{-1}) of Raman bands of the ground states of *E*-3, 4-d_2-HT and *E*-2, 5-d_2-HT excited at 514.5 and 317.5 nm.[a]

E-3, 4-d_2-HT		*E*-2, 5-d_2-HT
514.5 nm	317.5 nm	317.5 nm
1638		
1629		
1607p	1610	1618
1591		
1565p	1563	1570
1548		
1424		
1396p	1397	1381
1344		
1285p	1290	1214
1267		
1201p	1204	1295
1171		
1131		
1025		
1001p	1002	1022
954		
925		
901dp		
871p	871	
787dp		
558dp		
438p		
395		
360		
345p		
201dp		

[a] p polarized, dp depolarized.

ties before the transient experiments, and the ratio by GC of *E* to *Z* was 0.79/0.21 after the experiments of Fig. 2(B). The vibrational bands seen in Fig. 2(A) correspond to the strongest bands in the spectrum of Fig. 1; however, the relative intensities are changed due to preresonance with the optically allowed $1\,^1A_g \rightarrow 1\,^1B_u$ transition. In particular, the intensity of the C=C and C–C stretching bands at 1607 and 1201 cm^{-1} is strongly enhanced. This agrees with results on hexatriene-d_0 from the literature.[38] Three positive bands at 1320, 1132, and 897 cm^{-1} are observed in Fig. 2(B). Although the Raman spectrum of *Z*-3,4-d_2-HT is not known, on the basis of our previous results with hexatriene-d_0 we are confident to assign these bands to *Z*-3,4-d_2-HT. However, more caution is required in the C=C stretching region where bands from *E*-3,4-d_2-HT and *Z*-3,4-d_2-HT probably overlap.

Figure 3 shows preresonance Raman spectra for *E*-2,5-d_2-HT corresponding to Fig. 2. Unfortunately the amount of sample available was not sufficient to record the ordinary Raman spectrum of this compound with 514.5 nm excitation. The wave numbers of the strongest Raman bands observed in Fig. 3(A) are tabulated in Table I. The spectrum of Fig. 3(A) was obtained from an Ar-saturated solution of $\approx$5 mM *E*-2,5-d_2-HT in acetonitrile-d_0 and that of Fig. 3(B) from an Ar-saturated solution of 0.54 M acetone and $\approx$5 mM *E*-2,5-d_2-HT in acetonitrile-d_0 before and after irradiation with 2000 pump-and-probe pulses. In spectrum 3(B) negative bands are again seen at positions corresponding to ground state bands of *E*-2,5-d_2-HT and only one posi-

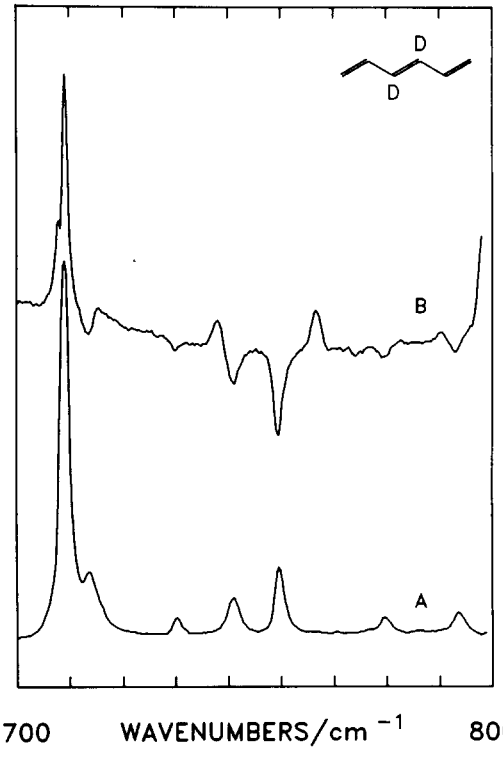

FIG. 2. Ground state (A) and difference (B) preresonance Raman spectra of *E*-3,4-d_2-1,3,5-hexatriene in Ar-saturated CD_3CN solution excited at 317.5 nm. A: $\approx$9 mM *E*-3,4-d_2-HT; B: 0.54 M acetone and $\approx$9 mM *E*-3,4-d_2-HT after 2000 pump-and-probe pulses. Solvent and acetone bands subtracted.

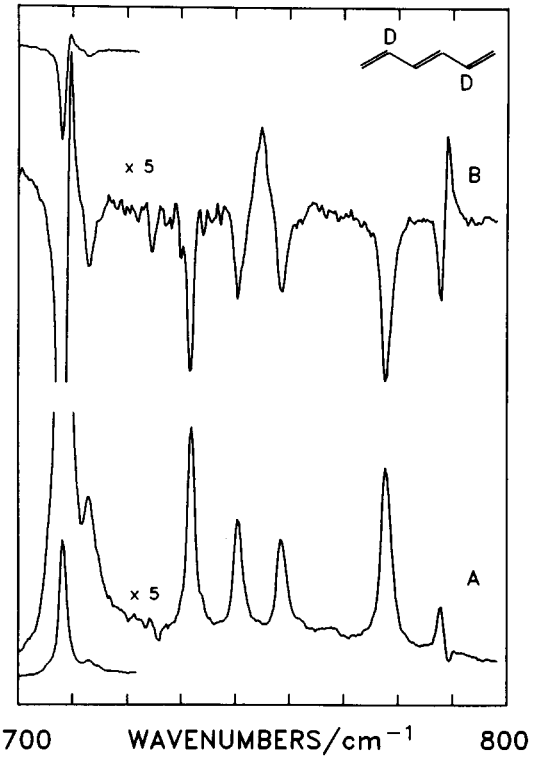

FIG. 3. Ground state (A) and difference (B) preresonance Raman spectra of *E*-2,5-d_2-1,3,5-hexatriene in Ar-saturated CH_3CN solution excited at 317.5 nm. A: $\approx$5 mM *E*-2,5-d_2-HT; B: 0.54 M acetone and $\approx$5 mM *E*-2,5-d_2-HT after 2000 pump-and-probe pulses.Solvent and acetone bands subtracted.

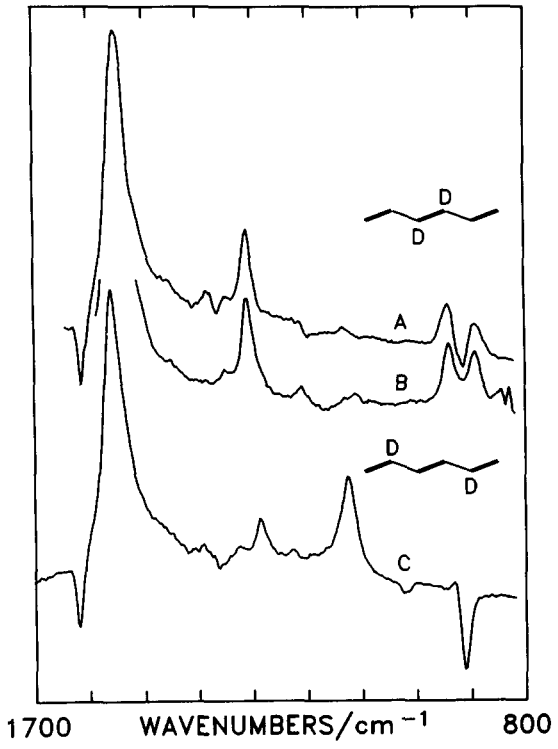

FIG. 4. Triplet state time-resolved resonance Raman spectra of Ar-saturated solutions of 0.54 M acetone and A: ≈5 mM *E*-3,4-d_2-HT in CH_3CN, B: ≈9 mM *E*-3,4d_2-HT in CD_3CN, and C: ≈5 mM *E*-2,5-d_2-HT in CH_3CN. Solvent, acetone, and hexatriene ground state bands subtracted. Excitation wavelength 317.5 nm, pump-probe delay 60 ns.

tive band is observed at 1252 cm^{-1} and assigned to *Z*-2,5-d_2-HT. Again, GC analysis showed no isomeric impurities before the transient experiments, and the ratio of *E* to *Z* by GC was 0.68/0.32 after the experiments of Fig. 3(B).

B. Excited triplet state

The spectra of *E*-3,4-d_2-HT and *E*-2,5-d_2-HT in their lowest excited triplet states obtained with a time delay of 60 ns between pump and probe pulses and excited at 317.5 nm are shown in Fig. 4. The corresponding wave numbers are tabulated in Table II together with previous data for hexatriene-d_0. Spectrum 4(A) was obtained from an Ar saturated solution of 0.54 M acetone and ≈5 mM *E*-3,4-d_2-HT in acetonitrile-d_0, spectrum 4(B) from an Ar-saturated solution of 0.54 M acetone and ≈9 mM *E*-3,4-d_2-HT in acetonitrile-d_3 and spectrum 4(C) from an Ar-saturated solution of 0.54 M acetone and ≈5 mM *E*-2,5-d_2-HT in acetonitrile-d_0. Acetonitrile-d_3 was used as solvent in some experiments in order to establish the presence of transient bands in regions masked by strong solvent bands from acetonitrile-d_0. All spectra shown in Fig. 4 are spectra after the subtraction of solvent bands and bands from ground state hexatriene obtained by procedures described in detail previously.[34] Such subtraction procedures can introduce negative bands due to the wavelength dependence of transient absorption. Such a band is seen in spectrum 4(C) at 917 cm^{-1}, the position of a strong band from acetonitrile-d_0.

Outside the region shown in Fig. 4, spectra were recorded down to 300 cm^{-1}, but no additional transient bands were found.

The isomeric purity of the samples was monitored throughout the experiments. The amount of *Z* isomers formed in the experiments underlying Fig. 4 was determined by GC before and after the experiments. The ratio of *E* to *Z* was 1.00/0.00 before the experiments, whereas after the experiments it was 0.96/0.04 for spectra 4(A) and 4(B) and 0.93/0.07 for spectrum 4(C). Hence the average isomeric purity of the samples was better than 96% during the recording of the triplet state resonance Raman spectra.

TABLE II. Wave numbers (cm^{-1}) of Raman bands of EHT-d_0, *E*-3, 4-d_2-HT, and *E*-2, 5-d_2-HT in the T_1 state.

EHT-d_0 in CH_3CN	*E*-3, 4-d_2-HT in CH_3CN	*E*-3, 4-d_2-HT in CD_3CN	*E*-2, 5-d_2-HT in CH_3CN
1570 vs	1551 vs	1551 vs	1560 vs
1270 s		1352 w	1326 w
1234 w	1310 s	1309 s	1286 m
1200 m		1209 w	1226 w
1106 s	937 m	939 m	1140 sh
	890 m	891 m	1123 s

IV. CALCULATIONS

A. Methods of calculation

Equilibrium geometries, normal coordinates, and vibrational frequencies were computed by the QCFF/PI program[39,40] which has been shown to be quite reliable in describing conjugated and aromatic systems.[13,14,41–43] With respect to the original program we have introduced the following modifications:

(a) Energies, gradients, and hessians of ground and excited states were computed by use of a general CI procedure including multiple excitations.[44] Since the original QCFF/PI program was based on CI limited to singly excited configurations (SECs) with respect to the closed shell ground configuration, a number of changes had to be introduced in the routines computing energy gradients and hessians. These modifications are very similar to those introduced by Zerbetto[45] in the upgrading of QCFF/PI with a CI procedure comprising SECs and doubly excited configurations (DECs) with respect to a closed shell configuration.

(b) In the computation of energy gradients and hessians we have included the off-diagonal elements of the HF matrix, F_{ij}, expressed in the MO basis. These matrix elements vanish, when the MOs are obtained by the SCF treatment. For this reason they have been neglected in the original program.[39,40] However, although the F_{ij} elements vanish for SCF MOs, their gradients do not. Hence their inclusion is necessary to obtain correct analytical gradients of excited electronic states.

(c) To compute energy gradients and hessians, the energy of the *N*th electronic state is expressed as[39,40]

$$V_N = \sum_r (R_r^{\alpha}\alpha_r + R_r^{\gamma}\gamma_{rr}) + \sum_{r\neq s}(R_{rs}^{\beta}\beta_{rs} + R_{rs}^{\gamma}\gamma_{rs}), \quad (1)$$

where *r* and *s* label atomic orbitals, α and β represent core integrals and γ Coulomb integrals, and *R* are coefficients

depending on the CI and MO coefficients. In the QCFF/PI program the hessian of this energy is computed analytically under the assumption that the coefficients R are constant. In this way the hessian of V_N is computed very efficiently but not entirely correctly. To take the derivatives of these coefficients into account, Warshel and Karplus[39] introduced a correction based on the polarizability theory in the MO scheme.[46] This correction leads to a correct force field for the (closed shell) ground state but is not satisfactory for excited states.

A straightforward procedure of computing the hessian of the energy V_N is numerical differentiation. Unfortunately this has the disadvantage of being tedious and in many cases unpracticable. However, we have noted that the gradients of V_N computed analytically, under the assumption of constant coefficients R, are quite close to the numerical gradients. Hence we have adopted the procedure of computing the hessian of V_N by numerical differentiation of analytical gradients. With this procedure we have been able to compute correctly the S_1 excited state frequencies of polyenes, benzene, and naphthalene.[47]

Normal coordinates were computed by diagonalization of the mass weighted Cartesian force constant matrix. Correlation between normal modes of different isotopic species is made by computing the rotation matrix relating the normal coordinates of the two species.

The calculations on triplet states were performed by the half-electron SCF Hamiltonian[48] followed by a CI calculation in which all singly excited determinants (SEDs) with respect to the lowest triplet, belonging to the $\pi\pi^*$ space, were considered. This CI includes 33 $\pi\pi^*$ triplet determinants.

Electronic energies and wave functions were computed by the SCF and CI procedures outlined above, both with the QCFF/PI and the CNDO/S[49] Hamiltonian.

B. Results

1. Ground state

A large number of calculations of the equilibrium geometry and force field of *E*- and *Z*-hexatriene have been performed using *ab initio*,[7-10] CNDO,[20] and QCFF/PI Hamiltonians.[13,14] These calculations, together with the classical observations by Lippincott *et al.*[17,18] and the more recent studies by Sabljič and McDiarmid[24] and Langkilde *et al.*[25] provide a reliable assignment of the infrared and Raman spectra of these compounds.

In this section we present the results of QCFF/PI calculations of equilibrium geometry and vibrational frequencies of 1,3,5-hexatriene and its 3,4-d_2- and 2,5-d_2-deuteriated derivatives. On the one hand, on the basis of these calculations we can assign the Raman spectra of the two deuteriated species shown in Sec. III. On the other hand, the comparison of observed and calculated wave numbers of the three isotopic species is a valuable test to assess the reliability of the computed force fields.

Beside their interest *per se*, ground state force fields, frequencies, and normal modes are a natural reference for the force fields, frequencies, and normal modes of the lowest triplet state T_1. For this reason we have performed the ground state calculations at the SCF level, without inclusion of interactions with doubly excited configurations (the contribution of singly excited configurations is automatically included in the SCF treatment), since T_1 calculations are based on a CI limited to singly excited configurations with respect to the dominant, HOMO–LUMO, configuration of the state T_1.

TABLE III. Geometry of the hexatriene carbon skeleton in the ground state S_0, the triplet state T_1, and the triplet state T_n ($n = 5$ or 6), (bond lengths in Å).

State geometry		C_1C_2	C_2C_3	C_3C_4	$C_1C_2C_3$	$C_2C_3C_4$
S_0	E[a]	1.343	1.470	1.354	122.2°	121.8°
	E[b]	1.347	1.462	1.359	121.9°	121.6°
	E[c]	1.324	1.463	1.329	124.3°	124.0°
	E[d]	1.3407	1.4630	1.3454	124.1°	123.9°
	E[e]	1.3399	1.4520	1.3462	124.1°	124.0°
	E[f]	1.337	1.458	1.368	121.7°	124.4°
	Z[a]	1.343	1.471	1.355	121.8°	125.3°
	Z[g]	1.3290	1.4621	1.3366	123.49°	127.19°
	Z[h]	1.336	1.462	1.362	122.13°	125.94°
T_1	E[a]	1.397	1.386	1.470	122.5°	121.5°
	Z[a]	1.397	1.387	1.472	122.0°	124.8°
	Tw[a]	1.384	1.388	1.480	122.6°	121.5°
T_n	$E(n=5)$[a]	1.410	1.428	1.415	121.2°	121.4°
	$Z(n=5)$[a]	1.411	1.432	1.412	121.2°	123.9°
	$\mathrm{Tw}(n=6)$[a]	1.411	1.415	1.470	121.2°	121.0°

[a] This work.
[b] Reference 14 (b) (theory).
[c] References 8 and 11 (theory).
[d] Reference 9 (theory).
[e] Reference 10 (theory).
[f] Reference 15 (expt.).
[g] Reference 7 (theory).
[h] Reference 16 (expt.).

a. E-hexatriene. The computed ground state geometry of the carbon skeleton is reported in Table III together with the results of other calculations and with experimental parameters. The numbering of the atoms is given in Fig. 5. The agreement between our calculations and the experimental results is satisfactory. This is especially true for the values of the CCC angles. The terminal C=C bonds are correctly predicted to be shorter than the central C=C bond.

The QCFF/PI force field, computed with respect to Cartesian coordinates, was transformed into a force field expressed in terms of the internal coordinates defined in Table

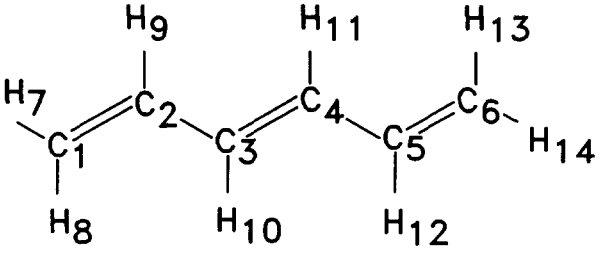

FIG. 5. Numbering of atoms in 1,3,5-hexatriene.

TABLE IV. Definition of internal coordinates.

No.	Type	Definition
1	CC stretch	C_1C_2
2	CC stretch	C_2C_3
3	CC stretch	C_3C_4
4	CC stretch	C_4C_5
5	CC stretch	C_5C_6
6	vinyl CH rock	$-C_1C_2H_9+C_3C_2H_9$
7	trans CH rock	$-C_2C_3H_{10}+C_4C_3H_{10}$
8	trans CH rock	$-H_{11}C_4C_5+C_3C_4H_{11}$
9	vinyl CH rock	$-C_6C_5H_{12}+C_4C_5H_{12}$
10	CH_2 scissor	$2H_7C_1H_8-H_7C_1C_2-H_8C_1C_2$
11	CH_2 scissor	$2H_{13}C_6H_{14}-H_{13}C_6C_5-H_{14}C_6C_5$
12	CH_2 rock	$-H_7C_1C_2+H_8C_1C_2$
13	CH_2 rock	$-H_{14}C_6C_5+H_{13}C_6C_5$
14	CCC terminal	$C_1C_2C_3$
15	CCC central	$C_2C_3C_4$
16	CCC central	$C_3C_4C_5$
17	CCC terminal	$C_4C_5C_6$
18	CH_2 twist	$H_8C_1C_2C_3+H_8C_1C_2H_9+H_7C_1C_2C_3+H_7C_1C_2H_9$
19	C–C torsion	$C_1C_2C_3H_{10}+C_1C_2C_3C_4+H_9C_2C_3H_{10}+H_9C_2C_3C_4$
20	C–C torsion	$H_{10}C_3C_4C_5+H_{10}C_3C_4H_{11}+C_2C_3C_4C_5+C_2C_3C_4H_{11}$
21	C–C torsion	$C_3C_4C_5H_{12}+C_3C_4C_5C_6+H_{11}C_4C_5H_{12}+H_{11}C_4C_5C_6$
22	CH_2 twist	$H_{12}C_5C_6H_{14}+H_{12}C_5C_6H_{13}+C_4C_5C_6H_{14}+C_4C_5C_6H_{13}$
23	CH_2 wag	$H_8H_7C_1C_2$
24	vinyl CH wag	$C_1H_9C_2C_3$
25	trans CH wag	$C_2H_{10}C_3C_4$
26	trans CH wag	$C_3H_{11}C_4C_5$
27	vinyl CH wag	$C_4H_{12}C_5C_6$
28	CH_2 wag	$C_5H_{13}C_6H_{14}$

IV. Such a force field is reported in Table V (in-plane coordinates) and in Table VI (diagonal force constants of out-of-plane coordinates). This force field is, as expected, very similar to the force field obtained recently by Karplus and co-workers[14(b)] by the same Hamiltonian, but with the inclusion of doubly excited configurations in the CI. This force field agrees essentially with a scaled *ab initio* SCF force field at the 6/31G and 4/21G levels.[7,9] The small differences are due to the overestimation by QCFF/PI of the interaction of adjacent CC stretchings and of the diagonal force constants of CCC bendings. The corresponding force field for the T_1 state (discussed below) is given in Table VII.

The CH_2 rock and, to a lesser extent, CH_2 scissor vibrations are weakly coupled to other coordinates. CH_2 scissoring is coupled only to C=C stretching; the main coupling of the CH_2 rock is to vinyl CH rock. CH rock is coupled both to C=C and C–C stretch. The force field is useful in understanding the changes in wave numbers and normal coordinates caused by deuteriation.

In Tables VIII and IX we report our computed wave numbers together with some of the previous theoretical results[7,9,10,14(b)] and with the most recent experimental

TABLE V. The in-plane force field of *E*-hexatriene in the S_0 state (CH stretch force constants omitted). Units are mdyn/Å for diagonal stretch constants and stretch–stretch interactions, mdyn Å/rad^2 for diagonal bend or torsion constants and bend–bend interactions, and mdyn/rad for stretch–bend interactions.

1	8.88																
2	0.62	5.42															
3	−0.08	0.60	8.50														
4	0.01	−0.02	0.60	5.42													
5	−0.01	0.01	−0.08	0.62	8.88												
6	−0.16	0.20	0.02	..	..	0.53											
7	−0.02	−0.20	0.19	0.02	..	−0.02	0.55										
8	..	0.02	0.19	−0.20	−0.02	0.01	0.02	0.55									
9	..	..	0.02	0.20	−0.16	..	0.01	−0.02	0.53								
10	−0.20	−0.01	..	..	..	..	..	..	...	0.46							
11	..	..	..	−0.01	−0.20	..	..	..	..	..	0.46						
12	0.02	0.02	..	..	..	−0.04	−0.01	..	..	−0.01	..	0.52					
13	..	..	..	0.02	0.02	..	..	−0.01	−0.04	..	−0.01	..	0.52				
14	0.22	0.20	−0.01	..	..	−0.01	..	..	..	−0.02	..	−0.04	..	1.37			
15	−0.01	0.21	0.21	−0.02	..	..	..	..	..	..	..	..	..	0.03	1.39		
16	..	−0.02	0.21	0.21	−0.01	..	..	..	..	..	..	..	..	..	0.03	1.39	
17	..	..	−0.01	0.20	0.22	..	..	..	..	..	−0.02	..	−0.04	..	..	0.03	1.37

TABLE VI. The out-of-plane diagonal force constants of hexatriene in the *E*, *Z*, and twisted (Tw) geometry and in the S_0 and T_1 states. (Units see Table V.)

	E, S_0	Z, S_0	E, T_1	Tw, T_1	Z, T_1
18	0.14	0.14	0.08	0.10	0.08
19	0.03	0.03	0.10	0.09	0.09
20	0.13	0.12	0.03	0.03	0.02
21	0.03	0.03	0.10	0.09	0.09
22	0.14	0.14	0.08	0.10	0.08
23	0.18	0.18	0.12	0.13	0.12
24	0.23	0.22	0.24	0.25	0.24
25	0.22	0.24	0.17	0.15	0.19
26	0.22	0.24	0.17	0.15	0.19
27	0.23	0.22	0.24	0.25	0.24
28	0.18	0.18	0.12	0.13	0.12

data.[24,25] The assignment given is qualitative and indicates the main components; in fact all the modes result from mixing of many internal coordinates, in particular the modes assigned as CH rock and C–C stretch. All theoretical calculations are in substantial agreement with each other.

The experimental assignments are in large part confirmed by calculations. There is a discrepancy between McDiarmid and Sabljic[24] and Langkilde *et al.*[25] in the assignment of CH_2 rock (b_u) and CH_2 wag (b_g). All the calculations are concordant in the following points: the frequency of CH_2 rock (b_u) is about 950 cm^{-1} and that of CH_2 wag (b_g) is higher than that of the lowest CH wag (b_g) and certainly higher than 900 cm^{-1}.

In Table X we report the wave numbers and the dominant components of the normal modes of EHT-d_0, *E*-3,4-d_2-HT, and *E*-2,5-d_2-HT. The correlation between the wave numbers of different isotopomers is drawn on the basis of the rotation matrix between the modes of the respective isotopomers.

Deuteriation changes the wave numbers of CH rock and CH wag vibrations. Hence it modifies both in-plane and out-of-plane normal modes. The mixed character of the in-plane modes with wave numbers in the region 1172–1350 cm^{-1} is seen by comparing with the corresponding modes of the deuteriated compounds, where a change of the dominant contributions is observed.

Upon deuteriation in positions 3,4, one of the a_g CH rock wave numbers drops to 1003 cm^{-1}, i.e., below the wave number of the C–C stretch, which is then pushed upwards compared to EHT-d_0 by the interaction with the 1003 cm^{-1} mode. The other CH rock remains nearly unchanged. The 1003 cm^{-1} mode gets close to the position of the CH_2 rock mode and pushes it down in wave number.

Similar effects are observed for the b_u modes as well. The CH rock at 1310 cm^{-1} is lowered upon 3,4-deuteriation to 1034 cm^{-1} and by near-resonant interaction pushes the CH_2 rock vibration from 946 to 896 cm^{-1}.

Among the out-of-plane modes, the only significant change noted is the lowering of one of the CH wags, namely of the a_u mode at 990 cm^{-1} and the b_g mode at 858 cm^{-1}.

Essentially similar effects are observed for *E*-2,5-d_2-HT. Among the a_g modes, that at 1305 cm^{-1} (CH rock) is lowered to 1027 cm^{-1}, which in turn pushes the CH_2 rock down from 941 to 864 cm^{-1}. Among the b_u modes, the CH rock at 1289 cm^{-1} is lowered to a value below 1000 cm^{-1} and interacts strongly with the CH_2 rock mode. At the same time, the mode at 1172 cm^{-1} which is predominantly C–C stretch is pushed up to 1214 cm^{-1} by interaction with the CH_2 and CD rocks. As far as the out-of-plane modes are concerned, the effect of deuteriation is simply that of decreasing the CH wag frequencies.

b. Z-hexatriene. Computed and experimental geometries of *Z*-hexatriene are reported in Table III. The QCFF/PI computed geometry is in good agreement with experiment.[16]

The force field of *Z*-hexatriene appears very similar to that of *E*-hexatriene and is not given here. The main difference is a higher value of the two central CCC bending force constants and of the coupling between them.

In Table IX we report the computed in-plane and out-of-plane wave numbers together with the results of previous theoretical work[7,14(b)] and with the most recent spectroscopic observations.[24,25] As can be seen from the tables, our results are in substantial agreement with those of the two previous calculations. Experimental assignments appear in

TABLE VII. The in-plane force field of *E*-hexatriene in the T_1 state (CH stretch force constants omitted).

1	5.97																
2	1.33	6.76															
3	0.25	0.48	5.06														
4	−0.24	0.13	0.48	6.76													
5	0.36	−0.24	0.25	1.33	5.97												
6	−0.17	0.19	0.02	··	··	0.53											
7	−0.02	−0.19	0.20	0.02	··	0.02	0.55										
8	··	0.02	0.20	−0.19	−0.02	0.01	0.02	0.55									
9	··	··	0.02	0.19	−0.17	··	0.01	−0.02	0.53								
10	−0.20	−0.01	··	··	··	··	··	··	···	0.45							
11	··	··	··	−0.01	−0.20	··	··	··	··	··	0.45						
12	0.02	0.02	··	··	··	−0.04	··	··	··	−0.01	··	0.52					
13	··	··	··	0.02	0.02	··	··	··	−0.04	··	−0.01	··	0.52				
14	0.20	0.19	−0.02	··	··	−0.01	··	··	··	−0.02	··	−0.04	··	1.36			
15	−0.01	0.21	0.20	−0.01	··	··	··	··	··	··	··	··	··	0.03	1.38		
16	··	−0.01	0.20	0.21	−0.01	··	··	··	··	··	··	··	··	··	0.04	1.38	
17	··	··	−0.02	0.19	0.20	··	··	··	−0.01	··	−0.02	··	−0.04	··	··	0.03	1.36

TABLE VIII. Computed and experimental vibrational wave numbers (cm^{-1}) of *E*-hexatriene in the S_0 state.

	This work	HBK[a]	FSLBP[b]	BPKP[c]	SKL[d]	Expt.[e]	Expt.[f]
a_g	1664 C=C	1619	1662	1664	1644	1623	1627
	1594 C=C	1577	1583	1559	1578	1574	1579
	1419 CH_2 sciss	1413	1414	1410	1403	1397	1400
	1350 CH rock	1350	1313	1299	1310	1288	1320
	1305 CH rock	1294	1288	1267	1292	1283	1288
	1206 C–C	1192	1198	1193	1202	1188	1192
	941 CH_2 rock	931	926	932	934	930	934
	461 CCC bend	457	432	429	443	444	449
	393 CCC bend	375	340	346	357	353	355
b_u	1645 C=C	1617	1634	1618	1626	1629	1629
	1445 CH_2 sciss	1463	1445	1449	1438	1433	1432
	1310 CH rock	1302	1301	1298	1296	1296	1295
	1289 CH rock	1271	1270	1235	1269	1255	1255
	1172 C–C	1179	1126	1121	1127	1132	1186
	946 CH_2 rock	944	957	953	958	966	1129
	589 CCC bend	578	530	536	553	541	543
	179 CCC bend	175	143	146	151	152	···
a_u	1082 CH wag	1057	1026	1015		1008	1013
	990 CH wag	961	953	948		938	937
	949 CH_2 wag	943	922	916		900	901
	643 C=CH_2 twist	619	679	677		683	683
	241 C=C twist	242	242	234		248	(317)
	101 C–C twist	106	94	88		94	90
b_g	1050 CH wag	1020	1000	995		985	988
	952 CH_2 wag	948	929	925		901	872
	858 CH wag	829	874	870		868	906
	611 C=CH_2 twist	594	590	582		428	433
	214 C–C twist	228	211	189		215	217

[a] Reference 14(b), PPP-DCI calculation.
[b] Reference 9, scaled force field from *ab initio* 4-21 G calculation.
[c] Reference 7, scaled force field from *ab initio* 6-31 G calculation.
[d] Reference 10, scaled force field from *ab initio* TZ + P calculation.
[e] Reference 25, experimental.
[f] Reference 24, experimental.

general to be consistent with each other and with those proposed by calculations. Two small discrepancies are noted. One pertains to the CH rock modes of b_1 type, the lowest of which is assigned to the 1187 cm^{-1} band by Langkilde *et al.*,[25] but to the 1280 cm^{-1} band by Sabljic *et al.*[24] This band is predicted theoretically to be close to or above 1300 cm^{-1}, which is more compatible with the assignment of Sabljic *et al.* In the b_2 species, the theoretical results concur with the assignment of CH and CH_2 wags of Langkilde *et al.* rather than with that of Sabljic *et al.*

The vibrational wave numbers and assignments of *Z*-hexatriene and of its 3,4- and 2,5-deuteriated isomers are given in Table XI. The effects of deuteriation are essentially limited to the region 1100–1400 cm^{-1} of the C–C stretches and CH rocks and to the CH wags. Furthermore, deuteriation induces a substantial rotation of the modes. These effects are similar to those found for the *E* isomer.

The experimentally observed wave numbers for the *Z* isomers of 3,4-d_2-HT and 2,5-d_2-HT (*vide supra*) can be compared with the calculated positions of a_1 modes. For *Z*-3,4-d_2-HT the modes at 1320, 1132, and 897 cm^{-1} are assigned to the calculated bands at 1324, 1170, and 899 cm^{-1}, respectively, and for *Z*-2,5-d_2-HT the mode at 1252 cm^{-1} is assigned to the calculated one at 1268 cm^{-1}.

2. Lowest triplet state T_1

In this section we report the computed equilibrium geometries, force fields, and vibrational wave numbers of hexatriene and its deuteriated isomers in the *E*, *Z* and twisted (Tw) forms in the lowest triplet state T_1. The corresponding experimental results for hexatriene-d_0 have been published previously[35] and those for the 3,4- and 2,5-dideuteriated hexatrienes are given in Sec. III of this paper.

The potential energy curve for the twisting around the central C=C bond (coordinate φ) in the ground state exhibits typically a high barrier ($\approx$50 kcal/mol) at the geometry $\varphi = 90°$. This is the basis for the existence of two distinct and stable forms, *E* and *Z*, in the ground state at room temperature. In the T_1 state the potential energy curve along φ is rather flat. This is a well known feature, that applies to all the ethylene derivatives and can be shown by Woodward–Hoffmann correlation diagrams. If the T_1 potential energy sur-

TABLE IX. Computed and experimental vibrational wave numbers (cm^{-1}) of *Z*-hexatriene in the S_0 state.

	This work	HBK[a]	BPKP[b]	Expt.[c]	Expt.[d]
a_1	1664 C=C	1619	1646	1623	1643
	1585 C=C	1565	1549	1578	1540
	1424 CH_2 sciss	1423	1411	1397	1398
	1330 CH rock	1325	1322	1315	1320
	1254 CH rock	1241	1239	1246	1249
	1120 C–C	1118	1078	1082	1084
	882 CH_2 rock	884	859	884	885
	422 CCC bend	417	384	394	393
	199 CCC bend	201	164	170	182
b_1	1642 C=C	1615	1612	1623	1623
	1465 CH_2 sciss	1468	1455	1450	1451
	1399 CH rock	1397	1334	1278	···
	1303 CH rock	1297	1289	1187	1280
	1225 C–C	1217	1187	1138	1187
	944 CH_2 rock	937	943	954	(979)
	707 CCC bend	705	676	680?	(508)
	420 CCC bend	410	347	353	355
a_2	1072 CH wag	1049	1010	1032?	···
	987 CH wag	961	974	952	954
	949 CH_2 wag	943	921	907	···
	670 C=CH_2 twist	649	704	707	707
	362 C=C twist	350	326	332	335
	153 C–C twist	168	126	155	160
b_2	1046 CH wag	1017	997	989	990
	952 CH_2 wag	948	928	906	825
	777 CH wag	764	794	815	908
	615 C=CH_2 twist	597	572	585	586
	104 C–C twist	113	88	100	110

[a] Reference 14(b).
[b] Reference 7.
[c] Reference 25.
[d] Reference 24.

face has two minima separated by an energy barrier ΔE, the rate constant k for the process leading from one minimum to the other can be expressed as

$$k = \frac{k_b T}{h} e^{-\Delta E/k_b T}, \tag{2}$$

where k_b is the Boltzmann constant. At room temperature ($T = 298$ K), with a typical $\Delta E \leqslant 8$ kcal/mol, this results in $k \geqslant 8.36 \times 10^6\ s^{-1}$. Hence equilibration can take place within the lifetime (~ 100 ns[35]) of the T_1 state. Thus in T_1 HT molecules can be regarded as moving almost freely along φ between the *E* and the *Z* geometries and are distributed statistically among the different geometries according to the Boltzmann rule. This property is the basis for their ability to isomerize in T_1. The actual $T_1 \rightarrow S_0$ decay takes place close to the Tw geometry, where the T_1–S_0 energy gap is smallest; once on the top of the S_0 barrier the molecule must choose one of the two stable forms of the S_0 state, thus eventually undergoing isomerization. If in T_1 the Tw geometry has the lowest energy, then according to the Boltzmann rule this is the dominant species in T_1 and the decay $T_1 \rightarrow S_0$ is very fast. If on the other hand the Tw geometry has a (moderately) higher energy than the *E* and *Z* forms in the T_1 state, the latter two are the dominant species. The decay then will still take place from a geometry near the Tw geometry, albeit with a slower rate, due to the larger energy gap between T_1 and S_0 at the Tw geometry. It is thus important to establish the energies of these three key geometries and to examine how many minima are found on the T_1 potential energy curve along φ.

According to the QCFF/PI calculations, relative minima are found at the *E* and *Z* geometries. After geometry optimization the *Z* form and the Tw form are computed at 1.1 and 7.1 kcal/mol, respectively, above the energy of the *E* form. The force field and the normal coordinates were evaluated at the three geometries *E*, *Z* and Tw. Previous calculations of the T_1 energy curve include *ab initio*[3,4,12] work and a MINDO/3 study.[12] One of the *ab initio* calculations[3] leads to results similar to ours: there are small barriers between the *E* and *Z* geometries and the *E* and *Z* forms have almost the same energy. The other *ab initio* and the MINDO/3 calculation lead to somewhat different results indicating a minimum with an energy of -6[12] or -1.9 kcal/mol[4] at the Tw geometry. However, MINDO/3, like most NDO methods, is known to overestimate conjugation and thus to prefer twisted geometries.

Accepting our calculated energy differences, the full thermal equilibration among the three forms is established with a rate constant $k = 3.8 \times 10^7\ s^{-1}$ according to Eq. (2). Hence the equilibrium is established in a time of ~ 30 ns, a time considerably shorter than the lifetime (~ 100 ns[35]) of the T_1 state. The relative equilibrium populations corresponding to the calculated energies are 1, 0.16, and 10^{-5} for the *E*, *Z*, and Tw forms, respectively. These results will be discussed in Sec. V in the light of the experimentally observed resonance Raman spectra.

a. E-hexatriene. The computed equilibrium geometry of the *E* form in the T_1 state is given in Table III. No direct experimental parameters are available for comparison. The differences of bond lengths with respect to the ground state are in agreement with expectations based on the changes in bond orders. It is interesting to note that, while both the C_1–C_2 and the C_3–C_4 bonds lengthen, the lengthening of the latter is considerably larger. In T_1 all the CCC angles become similar, roughly equal to 121.5°. The force field is given in Tables VI (diagonal force constants only) and VII. The main changes with respect to the force field of S_0 are observed in the CC stretch submatrix. The diagonal elements have changed in agreement with the changes of bond length. However, the largest force constant is considerably smaller than its counterpart in S_0. The vicinal coupling between C_1=C_2 and C_2–C_3 has become larger and the coupling between C_2–C_3 and C_3=C_4 has decreased. At the same time the couplings between nonadjacent stretches, which are small in S_0, have all become sizable in T_1. Also twisting force constants have changed in the way suggested by the change in bond length: the force constants of the twistings around the bonds C_1=C_2 and C_3=C_4 have decreased, while the force constants of the twisting around C_2–C_3 has increased.

The computed vibrational wave numbers of *E*-hexatriene in the T_1 state and of its deuteriated forms are reported

TABLE X. Computed and experimental ground state wave numbers (cm^{-1}) of *E*-hexatriene and its dideuteriated forms.[a]

	EHT-d_0	*E*-3, 4-d_2-HT	Expt.[b]	*E*-2, 5-d_2-HT	Expt.[c]
a_g	1664 C=C	1647 C=C	1607	1651 C=C	1618
	1594 C=C	1577 C=C	1565	1592 C=C	1570
	1419 CH_2 sciss	1419 CH_2 sciss	1396	1403 CH_2 sciss	1381
	1350 CH rock	1255 C–C (CH rock)	1201	1343 CH rock	1295
	1305 CH rock	1303 CH rock	1285	1245 C–C (CH_2 rock)	1214
	1206 C–C	1003 CD (CH_2) rock	1001	1027 CD (CH_2) rock	1022
	941 CH_2 rock	879 CH_2 (CD) rock	871	864 CH_2 (CD) rock	
	461 CCC bend	449 CCC bend	438	442 CCC bend	
	393 CCC bend	390 CCC bend	345	389 CCC bend	
b_u	1645 C=C	1643 C=C		1630 C=C	
	1445 CH_2 sciss	1441 CH_2 sciss		1428 CH_2 sciss	
	1310 CH rock	1034 CD (CH_2) rock		1302 CH rock	
	1289 CH rock	1295 CH (CH_2, CD) rock		1214 C–C (CH_2 rock)	
	1172 C–C	1173 C–C (CH rock)		984 CH_2 (CD) rock	
	946 CH_2 rock	896 CH_2 (CD) rock		887 CD, CH_2 rock	
	589 CCC bend	560 CCC bend		582 CCC bend	
	179 CCC bend	177 CCC bend		175 CCC bend	
a_u	1082 CH wag	1052 CH wag		1031 CH wag	
	990 CH wag	750 CD wag		870 CD wag	
	949 CH_2 wag	949 CH_2 wag		952 CH_2 wag	
	643 C=CH_2 twist	641 C=CH_2 twist		624 C=CH_2 twist	
	241 C=C twist	238 C=C twist		218 C=C twist	
	101 C–C twist	100 C–C		99 C–C twist	
b_g	1050 CH wag	1048 CH wag		893 CH, CD wag	
	952 CH_2 wag	951 CH_2 wag	901	954 CH_2 wag	
	858 CH wag	765 CD wag	787	845 CD, CH wag	
	611 C=CH_2 twist	579 C=CH_2 twist	558	585 C=CH_2 twist	
	214 C–C twist	197 C–C twist	201	211 C–C twist	

[a] The correspondence between the modes of deuteriated forms and those of hexatriene-d_0 has been obtained from the normal modes rotation matrix. Only dominant contributions to normal modes are given; internal coordinates in parentheses are less important. The labeling C=C and C–C is that pertinent to the ground state.
[b] This work; 514.5 nm excitation.
[c] This work; 317.5 nm excitation.

in Table XII. We discuss first hexatriene-d_0, starting with the in-plane vibrations. We note a decrease in the frequencies of the CC stretching modes compared to S_0: they are roughly 1550, 1200, and 1150 cm^{-1} of a_g symmetry and 1430 and 1140 cm^{-1} of b_u symmetry. Some of these modes are in the range of the CH rock wave numbers and accordingly mix strongly with them. Also the mixing between the three types of CC stretches is extensive and much larger than in S_0: This is due to the larger off-diagonal matrix elements found in the force fields. The highest wave number mode of b_u symmetry corresponds to CH_2 scissoring rather than CC stretching. Among the out-of-plane modes, the CH_2 wag wave numbers are lower than those in S_0 by 200 cm^{-1}. As expected, the order of the wave numbers of C_2C_3 and C_3C_4 twists is reversed compared to S_0.

Deuteriation in positions 3,4 or 2,5 produces a lowering of one of the CH rocks with an extensive mixing of the five a_g normal modes in the region 1369–939 cm^{-1}, namely of the modes based on the two CH rocks, two CC stretches, and the CH_2 rock. The CD rock mixes heavily with the CH_2 rock in both deuteriated species.

The effects of deuteriation on out-of-plane modes depend on the position of the isotopic substitution. Deuteriation in the 3,4 positions causes a decrease of the 830 cm^{-1} (a_u) and 805 cm^{-1} (b_g) CH wag wave numbers to 661 and 683 cm^{-1}, respectively, without significant perturbations on the other modes. Deuteriation in the 2,5 positions lowers the CH wags and, as a consequence these modes couple strongly with the CH_2 wags.

b. Z-hexatriene. The computed equilibrium geometry of *Z*-hexatriene in T_1 is reported in Table III. Bond lengths are almost identical to those of *E*-hexatriene. In contrast, CCC angles are found to be slightly different and this is probably related to different nonbonded interactions in the two geometries.

The force field is very similar to that of *E*-hexatriene and is not shown here. The only differences, which are rather small, are limited to the CCC submatrix.

The computed vibrational wave numbers of *Z*-hexatriene-d_0 and the two deuteriated species of *Z*-hexatriene are given in Table XIII. For a_1 symmetry the dominant feature is the strongly mixed character of most of the planar vibra-

TABLE XI. Computed ground state wave numbers (cm^{-1}) of *Z*-hexatriene and its dideuteriated forms.[a]

	ZHT-d_0	*Z*-3, 4-d_2-HT	*Z*-2, 5-d_2-HT
a_1	1664 C=C	1653 C=C	1649 C=C
	1585 C=C	1572 C=C	1584 C=C
	1424 CH_2 sciss (CH rock)	1423 CH_2 sciss (CH rock)	1405 CH_2 sciss
	1330 CH rock	1324 CH rock	1268 CH rock, C–C
	1254 CH rock, C–C	1170 C–C	952 CD rock
	1120 C–C, CH rock	837 CD rock	1154 CH rock
	882 CH_2 rock	899 CH_2 rock	865 CH_2 (CD) rock
	422 CCC bend	421 CCC bend	418 CCC bend
	199 CCC bend	198 CCC bend	194 CCC bend
b_1	1642 C=C	1639 C=C	1627 C=C
	1465 CH_2 sciss	1411 CH_2 sciss	1459 CH_2 sciss
	1399 CH rock	1323 C–C (CCC bend)	1383 CH rock (CH_2 sciss)
	1303 CH rock	1273 CH rock, C–C	1032 CD (CH_2) rock
	1225 C–C (CH rock)	1077 CD, CH_2 rock	1248 C–C (CH_2 rock)
	944 CH_2 rock	881 CH_2 (CD) rock	841 CH_2 (CD) rock
	707 CCC bend	685 CCC bend	670 CCC bend
	420 CCC bend	406 CCC bend	410 CCC bend
a_2	1072 CH wag	1043 CH wag	1026 CH wag
	987 CH wag	801 CD wag	865 CD wag
	949 CH_2 wag	950 CH_2 wag	953 CH_2 wag
	670 CH_2=C (C=C) twist	648 CH_2 = C twist	656 CH_2=C twist
	363 C=C twist	338 C=C twist	349 C=C twist
	153 C–C twist	162 C–C twist	136 C–C twist
b_2	1046 CH wag	1044 CH wag	881 CH, CD wag
	952 CH_2 wag	952 CH_2 wag	954 CH_2 wag
	777 CH wag	666 CD wag, CH_2 = C twist	774 CD, CH wag
	615 CH_2=C twist	558 CH_2=C twist, CD wag	588 CH_2=C twist
	104 C–C twist	104 C–C twist	98 C–C twist

[a] See footnote a of Table X.

tions. In *Z*-hexatriene-d_0 the 1539 cm^{-1} band corresponds to a mixture of the different types of CC stretch. The four modes at 1331, 1290, 1207, and 1089 cm^{-1} correspond to a combination of the two CH rocks and the two CC stretches. Upon deuteriation the mixing involves the CH_2 rock as well, besides the four modes noted above. In the case of 2,5-d_2-HT even the CH_2 scissoring becomes involved in the mixing.

In the b_1 space, we notice the same kind of mixing of internal coordinates. Interestingly, the mode with highest wave number has C–C stretch and CH_2 scissor components and its dominant character depends on the specific substitution.

In the out-of-plane modes we notice the same features as in EHT.

c. Twisted hexatriene. The optimized geometry of Tw hexatriene is given in Table III. It can be seen that the carbon skeleton parameters are essentially similar to those of the *E* geometry. Small differences are the slightly longer central C_3–C_4 bond and the slightly shorter C_1–C_2 bond.

At the twisted geometry, the molecular symmetry group is C_2 and it is not possible to distinguish rigorously between in-plane and out-of-plane coordinates. However, since the interactions between formerly in-plane and out-of-plane coordinates are very small, the distinction is still practically feasible.

The "in-plane" force field (not shown here) is very similar to that of the *E* form. The main difference pertains to off-diagonal elements between CC stretch coordinates: here only the couplings between stretching of adjacent bonds are non-zero.

The computed vibrational wave numbers are reported in Table XIV. The highest wave number of "*a*" type is about 1500 cm^{-1}, that is, very similar to the wave number of CH_2 scissor. Hence the modes with the two highest wave numbers are mixed and are of CC stretch and CH_2 scissor parentage. Furthermore, similarly to the *E* and *Z* isomers, we notice extensive mixing among CC stretch and CH rocks. A difference with respect to the *E* and *Z* forms is the inversion of the order of the CH_2 wag and the lowest CH wag mode.

The effect of deuteriation is manifested in the lowering of a CH rock mode, which then mixes with a CH_2 rock mode, and in the lowering of a CH wag mode which mixes with CH_2 wag. The same comments hold for the "*b*"-type vibrations.

d. Rotation of normal coordinates, Duschinsky effect. The normal modes of T_1 are not the same as in S_0. Electronic excitation induces a mixing of coordinates, as it was first pointed out by Duschinsky.[51] The linear transformation relating the vibrational modes of S_0 and T_1 can be written as

$$Q^g = JQ^t + \Delta Q^g, \tag{3}$$

TABLE XII. Computed wave numbers (cm^{-1}) of *E*-hexatriene and its deuteriated forms in the T_1 state.[a,b]

	EHT-d_0	*E*-3, 4-d_2-HT	*E*-2, 5-d_2-HT
a_g	1554 C–C, C=C_c	1525 C–C, C=C_c	1539 C–C, C=C_c
	1483 CH_2 sciss	1479 CH_2 sciss (C=C)	1481 CH_2 sciss
	1369 CH rock (C=C)	1340 CH rock, C=C	1310 C=C (CCC bend)
	1321 CH rock (C–C, CCC bend)	1260 CH rock, CCC bend, C=C_c	1290 CH (CD) rock
	1193 C=C (C–C, CH rock)	964 CH_2, CD rock	1023 CH_2, CD rock
	1154 C=C_c (C=C)	1158 C=C_c, C=C	1153 C=C_c (C=C)
	939 CH_2 rock	896 CD, CH_2 rock	857 CD, CH_2 rock
	448 CCC bend	438 CCC bend	431 CCC bend
	385 CCC bend	381 CCC bend	382 CCC bend
b_u	1473 CH_2 sciss	1473 CH_2 sciss	1472 CH_2 sciss
	1430 CH rock, C–C	1413 CH rock, C–C (C=C)	1374 CH rock, C–C
	1323 CH rock (CCC bend)	1027 CD, CH_2 rock	1304 C–C, CH rock
	1243 CH rock, C–C	1258 C–C (C=C, CH rock)	1170 C=C (CD rock)
	1139 C=C (C–C)	1167 C=C (C–C)	1010 CH_2, CD rock
	963 CH_2 rock	907 CH_2, CD rock	879 CD, CH_2 rock
	599 CCC bend	567 CCC bend	592 CCC bend
	177 CCC bend	175 CCC bend	173 CCC bend
a_u	1032 CH wag	996 CH wag	898 CH (CH_2) wag
	830 CH wag	661 CD wag	780 CD, CH_2 wag
	757 CH_2 wag	769 CH_2 wag	737 CH_2, CD wag
	565 C=CH_2 twist	551 C=CH_2 twist	563 C=CH_2 twist
	193 C–C twist	186 C–C twist	173 C–C twist
	110 C=C twist	107 C=C twist	109 C=C twist
b_g	1012 CH wag	994 CH wag	883 CH (CH_2) wag
	805 CH wag	683 CD wag	785 CD, CH_2 wag
	754 CH_2 wag	767 CH_2 wag	745 CH_2, CD wag
	564 C=CH_2 twist	534 C=CH_2 twist	561 C=CH_2 twist
	297 C–C twist	285 C–C twist	295 C–C twist

[a] See footnote a of Table X.
[b] C=C_c denotes the central CC bond.

where Q^g and Q^t are the normal modes of S_0 and T_1, respectively, ΔQ^g is the displacement of T_1 equilibrium geometry projected on the S_0 normal coordinates and J is the rotation matrix expressing the Duschinsky effect.

To illustrate this, the calculated Duschinsky matrices for the a_g modes of the *E* isomers of hexatriene-d_0 and 3,4-d_0-HT in the T_1 state with respect to the S_0 state are given in Table XV. It can be seen that indeed a considerable rotation of normal coordinates takes place. This rotation is not limited to the region of strong mixing in the ground state (1000–1300 cm^{-1}) but includes the C=C stretching modes of the ground state around 1600 cm^{-1} and the scissoring modes at 1419 cm^{-1} as well. As a result of the Duschinsky effect, the mixing of internal coordinates is considerably more extensive in the normal coordinates of T_1 than in those of S_0. One of the effects of deuteriation is seen to be a partial decoupling of the CD rock mode (1003 cm^{-1} in S_0) from the other ones and consequently a considerably smaller rotation of this mode.

3. Electronic energies of triplet states

Computed electronic energies, wave functions, and oscillator strengths for the lowest triplet states are given in Tables XVI, XVII, and XVIII for the *E*, *Z*, and Tw forms. These calculations have been performed with both CNDO/S and QCFF/PI Hamiltonians. The results obtained by QCFF/PI are shown in Fig. 6. The geometries adopted were those of Table III, obtained by energy minimization.

The lowest triplet state T_1 is well described by a single configuration, namely the HOMO→LUMO (or 3→4) with respect to the ground configuration. The HOMO→LUMO configuration of *E*-hexatriene is considered the reference configuration, and in Tables XVI, XVII, and XVIII the other configurations are expressed relative to this reference. The energy of the T_1 state of *E*-hexatriene is found at 1.08 eV (24.9 kcal/mol) by QCFF/PI. It should be noted that experimentally the T_1–S_0 energy gap is found at 2.03 eV.[28,29] This underestimate of the T_1–S_0 energy gap is due to our choice of using a different CI for the T_1 and the S_0 states in order to treat the two states on equal footing as far as potential energy surfaces are concerned. QCFF/PI and CNDO/S are parametrized in order to give correct vertical energy gaps within the same CI. Using the same CI for S_0 and T_1 we find a vertical T_1–S_0 energy gap of 2.06 eV (QCFF/PI) and 2.33 eV (CNDO/S), in good agreement with the experimental results.

TABLE XIII. Computed wave numbers (cm^{-1}) of *Z*-hexatriene and its deuteriated forms in the T_1 state.[a]

	ZHT-d_0	*Z*-3, 4-d_2-HT	*Z*-2, 5-d_2-HT
a_1	1539 C–C, C=C_c (C=C)	1531 C–C, C=C_c, CH rock	1512 C–C, C=C_c, CH_2 sciss
	1475 CH_2 sciss	1475 CH_2 sciss	1470 CH_2 sciss (C–C)
	1331 CH rock (C=C_c)	1254 C=C (C–C, CCC bend)	1308 CH rock (C–C)
	1290 CH rock (C–C)	1294 CH rock, C=C_c	968 CD rock (C=C)
	1207 C=C (C=C_c, CH rock)	1160 C=C_c (C=C)	1212 C=C, C=C_c
	1089 C=C_c (CH_2, CH rock)	822 CD rock	1110 C=C_c, C=C, CH_2 rock
	893 CH_2 rock (C=C_c)	914 CH_2, CD rock	864 CH_2, CD rock
	416 CCC bend	415 CCC bend	411 CCC bend
	194 CCC bend	192 CCC bend	184 CCC bend
b_1	1504 C–C (CH_2 sciss)	1480 CH_2 sciss	1496 C–C (CH_2 sciss)
	1460 CH_2 sciss (C–C, C=C)	1427 C–C, CH rock	1456 CH_2 sciss (C–C, C=C)
	1362 CH rock (C=C)	1345 CH rock, C–C	1226 C=C (C–C, CD rock)
	1310 CH rock (C–C)	1173 C=C (CD rock)	1291 CH rock (CCC bend)
	1112 C=C (C–C, CH rock)	1042 CD, CH_2 rock	1006 CH_2 (CD) rock
	955 CH_2 rock	893 CH_2, CD rock	894 CD, CH_2 rock
	718 CCC bend	694 CCC bend	687 CCC bend
	405 CCC bend	392 CCC bend	395 CCC bend
a_2	1017 CH wag	991 CH wag	875 CH wag
	830 CH wag	693 CD (CH_2) wag	784 CD (CH_2) wag
	757 CH_2 wag	763 CH_2 (CD) wag	747 CH_2 (CD) wag
	575 C=CH_2 twist	549 C=CH_2 twist	575 C=CH_2 twist
	306 C–C twist	293 C–C twist	306 C–C twist
	143 C=C twist	136 C=C twist	127 C=C twist
b_2	1015 CH wag	992 CH wag	850 CH wag
	799 CH wag	766 CH_2 (CD) wag	777 CH_2, CD wag
	744 CH_2 wag	643 CD (CH_2) wag	729 CD, CH_2 wag
	556 C=CH_2 twist	538 C=CH_2 twist	554 C=CH_2 twist
	149 C–C twist	148 C–C twist	142 C–C twist

[a] See footnote a of Tables X and XII.

In the *E* form, the second triplet is found at ~2.2 eV above T_1 and the transition $T_1 \rightarrow T_2$ is very weakly allowed. From ~2.0 eV up to ~6.5 eV we find only one triplet state, T_5, with a large transition moment to T_1. This state is located at about 4.5 eV (4.32 eV with QCFF/PI and 4.69 eV with CNDO/S) above T_1. The T_5 state is obtained essentially by the same two configurations appearing in the wave functions of T_2 but with opposite phase. We wish to stress that the two methods used yield the same results and hence support each other. From the physical point of view these results are interesting, since they indicate that both transient absorption experiments and transient resonance Raman spectra of T_1 can be explained in terms of only one electronic transition, namely the $T_1 \rightarrow T_5$ transition. Essentially the same results have been obtained for the *Z* form.

At the Tw geometry the situation is somewhat different. In fact the system is composed of two allylic moieties interacting weakly and, accordingly, some of the excited states can be considered to be due to allylic excitations that are degenerate. The state with the largest oscillator strength to T_1 is T_6 computed to be at ~5.5 eV above T_1. This theoretical result is comparable with the experimentally found absorption spectrum for the allyl radical in an Ar matrix at 10 K.[50] A weak electronic absorption band was found at 408.5 nm and a strong one with a maximum at 213 nm, corresponding to energies of 3.03 and 5.81 eV, respectively. These values are rather close to the calculated values 3.40 and 5.49 eV (QCFF/PI) and 3.27 and 5.75 eV (CNDO/S). Hence at 90°, the state active in absorption and in resonance Raman scattering has shifted toward the far UV. Even for this geometry, CNDO/S and QCFF/PI methods yield equivalent results.

To get information on the energy of the lowest electronic states and in particular of the absorbing state, we have performed additional QCFF/PI calculations at angles $\varphi = 45°$ and $\varphi = 60°$ ($\varphi = 0°$ is the *E* form). From the results (not shown here) it appears that the energy gap between the lowest triplet and the absorbing state increases smoothly go-

TABLE XIV. Computed wave numbers (cm^{-1}) of 90° twisted (Tw) hexatriene and its deuteriated forms in the T_1 state.[a]

	HT-d_0	3, 4-d_2-HT	2, 5-d_2-HT
a	1497 C=C, C=C_c, C-C (CH_2 sciss)	1491 CH_2 sciss	1488 CH_2 sciss (C=C)
	1483 CH_2 sciss (C=C_c, C-C)	1472 C-C, C=C_c, CH rock	1459 C=C_c, C-C, CH rock
	1317 CH rock, C-C (C=C)	1310 C=C, C=C_c (C-C, CH rock)	1275 C=C, CH rock
	1309 CH rock (CCC bend)	1248 C=C_c (CH rock, CCC bend)	1285 C-C, C=C, CCC bend
	1192 C=C (C-C, CH rock)	1170 C=C, C=C_c (C-C)	999 CH_2, CD rock
	1136 C=C_c (CH rock)	886 CD rock	1135 C=C_c (CD rock)
	1035 CH wag	1022 CH wag	830 CD (CH_2) wag
	919 CH_2 rock	913 CH_2 rock	852 CD (CH_2) rock
	821 CH_2 wag	814 CH_2 wag	819 CH_2 wag
	731 CH wag	654 CD wag	726 CH wag
	582 C=CH_2 twist	542 C=CH_2 twist	575 C=CH_2 twist
	411 CCC bend	404 CCC bend	405 CCC bend
	367 CCC bend	352 CCC bend	360 CCC bend
	140 C-C twist	139 C-C twist	135 C-C twist
	− 168 C=C twist	− 166 C=C twist	− 153 C=C twist
b	1493 CH_2 sciss (C=C)	1491 CH_2 sciss	1488 CH_2 sciss (C=C)
	1460 C-C, CH rock	1442 C-C, CH rock	1425 C-C, CH rock
	1311 CH rock (C-C, CCC bend)	1053 CD (CH_2) rock	1287 CH rock, C-C
	1300 CH rock (C-C, C=C)	1296 C=C, C-C	1267 C=C (CH rock)
	1194 C=C, C-C (CH rock)	1212 CH rock (C=C, C-C)	1009 CH_2, CD rock
	1040 CH wag	1023 CH wag	846 CD, CH wag
	957 CH_2 rock	898 CH_2 (CD) rock	895 CD, CH_2 rock
	827 CH_2 wag	816 CH_2 wag	823 CH_2, CD wag
	779 CH wag	719 CD wag (CCC bend)	760 CD, CH_2 wag
	641 CCC bend (C=CH_2 twist)	548 C=CH_2 twist (CCC bend)	631 CCC bend (C=CH_2 twist)
	587 C=CH_2 twist (CCC bend)	579 CCC bend (C=CH_2 twist)	581 C=CH_2 twist (CCC bend)
	369 CCC bend	353 CCC bend	363 CCC bend
	155 C-C twist	154 C-C twist	148 C-C twist

[a] See footnote a of Tables X and XII.

ing from E to 45° and 60° geometries. However, even at $\varphi = 60°$ this energy gap is still closer to that to the E form than to that of the Tw form.

4. Activity of totally symmetric modes in transient resonance Raman spectra

In this section we wish to determine, on the basis of the present calculations, the most active modes in the resonance Raman scattering of the transient T_1 state with an exciting wavelength in the region 315–317.5 nm as reported previously.[35] At the same time we can identify the modes that are most prominent in the vibrational structure of the intense $T_1 \rightarrow T_n$ (with $n = 5$ in the E and Z forms and $n = 6$ in the Tw form) transition.

A wavelength of 315 nm corresponds to an energy of 3.94 eV. Since this energy is sufficiently close to the calculated energy gap of the intense $T_1 \rightarrow T_5$ transition, found to be at ~4.3 eV, the scattering tensor is dominated by the contribution of this strongly allowed transition, and the experimental wavelength corresponds to a resonance situation. Therefore, it is a good approximation to restrict our attention to this transition. In this case the most active modes are those gaining their scattering intensity from the Franck–Condon mechanism, namely the totally symmetric (TS) modes. Nontotally symmetric (NTS) modes, whose fundamentals gain intensity by vibronic coupling, are likely to show a relatively small activity.

The activity of TS modes may be due to displacement between the equilibrium geometries of T_1 and T_5, or to the difference between vibrational wave numbers in the two states. It is well known that displacement usually gives rise to a much larger Franck–Condon activity than wave number differences. In the case of hexatriene, according to QCFF/PI calculations the vibrational wave numbers in T_5 never differ from the wave numbers in T_1 by more than 4%; in most cases the difference is $\leqslant 1\%$. Hence displacement is by far the most important factor governing Franck–Condon factors. For simplicity we thus assume the wave numbers of vibrational modes to be equal in the two states and we consider only the contribution of displacement.

The parameter governing the contribution of displacement to the Franck–Condon factor is γ, which is the ratio

TABLE XV. Duschinsky matrices of the rotation of the totally symmetric vibration modes (a_g) upon excitation from S_0 to T_1.

		E-hexatriene-d_0 Triplet state T_1								
	ν	1554	1483	1369	1154	1321	1193	939	448	385
Ground state	1664	−0.86	0.32	−0.20	−0.10	−0.24	−0.18			
	1594	−0.21	−0.66	0.27	−0.61	−0.20	0.16			
	1419	−0.14	−0.63	−0.64	0.40					
	1350	0.35	0.19	−0.65	−0.62		−0.16			
	1305	0.24		0.12	0.20	−0.83	−0.44			
	1206		−0.12	0.22	−0.12	0.45	−0.84	−0.11		
	941				0.12			−0.98		
	461								−0.99	−0.10
	393								0.10	−0.99
		E-3, 4-d_2-hexatriene Triplet state T_1								
	ν	1525	1158	1479	1260	1340	964	896	438	381
Ground state	1647	−0.86	−0.12	0.34	−0.25	0.26				
	1577	−0.28	0.60	−0.60	−0.33	−0.22	0.18			
	1419	0.11	0.41	0.69	−0.19	−0.55				
	1303	0.38	−0.12		−0.84	0.34				
	1255	0.13	0.63	0.20	0.27	0.68				
	1003		−0.19		0.10		0.97			
	879							−0.99		
	449								−0.99	−0.11
	390								−0.11	0.99

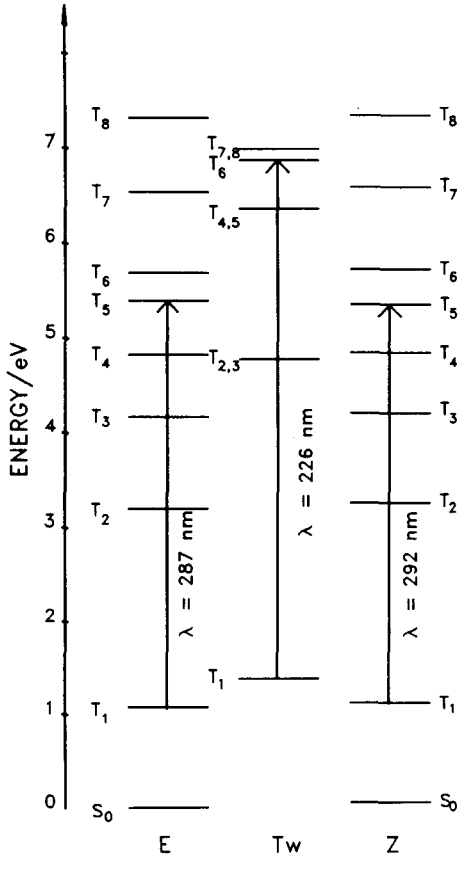

FIG. 6. Calculated energy level diagram for the triplet states of 1,3,5-hexatriene in the planar *E*, *Z*, and twisted (Tw) forms and the strongest optically allowed transitions.

between half of the Stokes shift and the vibrational quantum. Thus if $\mathbb{Q}_i$ (1) and $\mathbb{Q}_i$ (n) are the equilibrium geometries along the (mass-weighted) normal coordinates Q_i in the states T_1 and T_n, respectively, the parameter γ_i associated to Q_i is given by

$$\gamma_i = (\omega_i/2\hbar)[\mathbb{Q}_i(1) - \mathbb{Q}_i(n)]^2, \tag{4}$$

where ω_i is in rad/s. The parameter $\mathbb{Q}_i = [\mathbb{Q}_i(1) - \mathbb{Q}_i(n)]$ is simply the projection onto the normal coordinate Q_i of T_1 of the change of equilibrium Cartesian coordinates in the two states. That is, $\mathbb{Q}_i$ can be written as[13]

$$\mathbb{Q}_i = [\mathbf{x}(1) - \mathbf{x}(n)]\mathbf{M}^{1/2}\mathbf{L}_i(T_1), \tag{5}$$

where $\mathbf{x}(m)$ is the $3N$ dimensional vector of the equilibrium Cartesian coordinates in the state T_m, $\mathbf{M}$ is the $3N \times 3N$ diagonal matrix of the atomic masses and $\mathbf{L}_i$ is the $3N$ vector describing normal coordinates Q_i in terms of mass-weighted Cartesian coordinates.

We have computed the parameters γ_i for each TS normal coordinate at the *E*, *Z*, and Tw geometries and for the three isotopic species. The results are reported in Tables XIX, XX, and XXI. We consider first hexatriene-d_0.

In the *E* geometry the largest γ's are associated with the modes at 1554 and 1154 cm^{-1}; smaller γ's are found for the modes at 1369, 1321, and 447 cm^{-1}. In the *Z* geometry the largest γ's are due to the modes at 1539 and 1290 cm^{-1}; smaller values are found for the modes at 1475, 1207, and 194 cm^{-1}. At the Tw geometry the modes with the largest γ's are found at 1483, 1317, and 1309 cm^{-1}. The γ's for this geometry are smaller than the largest values found in the *E* and *Z* geometries. Hence the three geometries have each a

TABLE XVI. Relative energies (E, eV), wave functions, and $T_1 \rightarrow T_n$ oscillator strengths (f) for the lowest triplet states of E-hexatriene.

		CNDO/S		QCFF/PI		
	Type	E	f	E	f	Wave function
T_1	B_u	0.00	⋯	0.00	⋯	0.96 (ground)
T_2	A_g	2.25	0.01	2.12	0.00	$0.69(2\rightarrow3) + 0.63(4\rightarrow5)$
T_3	B_u	3.15	0.00	3.09	0.00	$-0.64(1\rightarrow3) + 0.58(4\rightarrow6)$
T_4	B_u	3.93	0.00	3.75	0.00	$-0.54(2\rightarrow4) - 0.51(2,4\rightarrow3,5) - 0.50(3\rightarrow5)$
T_5	A_g	4.69	0.60	4.32	0.85	$-0.67(2\rightarrow3) + 0.69(4\rightarrow5)$
T_6	A_g	4.77	0.32	4.61	0.01	$0.42(1\rightarrow4) + 0.47(1,4\rightarrow3,5) - 0.40(3\rightarrow6)$
T_7	B_u	6.25	0.00	5.46	0.00	$0.67(1\rightarrow3) + 0.71(4\rightarrow6)$
T_8	B_u	6.97	0.00	6.24	0.00	$0.76(2\rightarrow4) - 0.56(3\rightarrow5)$

[a] MOs are labeled in the order of increasing energy. We have included with singly excited configurations also excited configurations in which one excitation is internal to the half-occupied orbital space.

TABLE XVII. Relative energies (E, eV), wave functions, and $T_1 \rightarrow T_n$ oscillator strengths (f) for the lowest triplet states of Z-hexatriene.

		CNDO/S		QCFF/PI		
	Type	E	f	E	f	Wave functions[a]
T_1	B_2	0.00	⋯	0.00	⋯	0.96 (ground)
T_2	A_1	2.20	0.01	2.14	0.00	$0.68(2\rightarrow3) - 0.63(4\rightarrow5)$
T_3	B_2	3.14	0.01	3.09	0.00	$-0.65(1\rightarrow3) - 0.59(4\rightarrow6)$
T_4	B_2	3.87	0.01	3.73	0.00	$0.53(2\rightarrow4) + 0.54(2,4\rightarrow3,5) - 0.50(3\rightarrow5)$
T_5	A_1	4.57	0.61	4.24	0.66	$-0.67(2\rightarrow3) - 0.70(4\rightarrow5)$
T_6	A_1	4.75	0.07	4.61	0.01	$0.43(1\rightarrow4) + 0.41(3\rightarrow6)$
T_7	B_2	6.25	0.10	5.47	0.13	$0.67(1\rightarrow3) - 0.71(4\rightarrow6)$
T_8	B_2	6.96	0.09	6.23	0.04	$-0.77(2\rightarrow4) - 0.53(3\rightarrow5)$

[a] See footnote a of Table XVI.

TABLE XVIII. Relative energies (E, eV), wave functions, and $T_1 \rightarrow T_n$ oscillator strengths (f) for the lowest triplet states of 90° twisted (Tw) hexatriene.

		CNDO/S		QCFF/PI		
	Type	E	f	E	f	Wave functions[a]
T_1	B	0.00	⋯	0.00	⋯	0.97 (ground)
T_2	A	3.27	0.03	3.40	0.01	$0.55(2\rightarrow3) + 0.53(1\rightarrow4) + 0.46(4\rightarrow5) - 0.44(3\rightarrow6)$
T_3	B	3.34	0.00	3.40	0.00	$-0.53(2\rightarrow4) - 0.53(1\rightarrow3) + 0.47(4\rightarrow6) - 0.46(3\rightarrow5)$
T_4	B	5.40	0.00	4.98	0.00	$-0.42(2,4\rightarrow3,5) + 0.41(1,4\rightarrow3,6) + 0.40(2,3\rightarrow4,5)$
T_5	A	5.40	0.00	4.98	0.00	$0.42(1,4\rightarrow3,5) - 0.42(2,4\rightarrow3,6) - 0.40(1,3\rightarrow4,5)$
T_6	A	5.75	0.85	5.49	0.73	$-0.55(2\rightarrow3) - 0.34(1\rightarrow4) + 0.57(4\rightarrow5) - 0.50(3\rightarrow6)$
T_7	B	⋯	⋯	5.61	0.00	$-0.68(2\rightarrow4) + 0.68(1\rightarrow3)$
T_8	A	⋯	⋯	5.62	0.02	$0.59(2\rightarrow3) - 0.75(1\rightarrow4)$

[a] See footnote a of Table XVI.

TABLE XIX. Stokes shift parameters γ for the $T_1 \rightarrow T_5$ transition of totally symmetric normal modes (a_g) of E-hexatriene and its deuteriated forms.[a]

EHT-d_0		E-3, 4-d_2-HT		E-2, 5-d_2-HT	
ν (cm^{-1})	γ	ν (cm^{-1})	γ	ν (cm^{-1})	γ
1554	0.24	1525	0.24	1539	0.27
1483	0.04	1479	0.08	1481	0.04
1369	0.05	1340	0.18	1310	0.06
1321	0.06	1260	0.01	1290	0.04
1193	0.03	964	0.04	1023	0.02
1154	0.25	1158	0.07	1153	0.28
939	0.01	896	0.08	857	0.00
447	0.06	438	0.04	431	0.06
385	0.04	381	0.04	382	0.05

[a] Computed by QCFF/PI.

TABLE XX. Stokes shift parameters γ for the $T_1 \rightarrow T_5$ transition of totally symmetric normal modes (a_1) of Z-hexatriene and its deuteriated forms.[a]

ZHT-d_0		Z-3, 4-d_2-HT		Z-2, 5-d_2-HT	
ν (cm^{-1})	γ	ν (cm^{-1})	γ	ν (cm^{-1})	γ
1539	0.21	1531	0.22	1512	0.21
1475	0.06	1475	0.07	1470	0.14
1331	0.00	1254	0.22	1308	0.07
1290	0.37	1294	0.22	968	0.02
1207	0.11	1160	0.06	1212	0.32
1089	0.04	822	0.00	1110	0.06
893	0.03	914	0.04	864	0.01
416	0.04	415	0.04	411	0.04
194	0.10	192	0.10	189	0.10

[a] Computed by QCFF/PI.

TABLE XXI. Stokes shift parameters γ for the $T_1 \rightarrow T_6$ transition of totally symmetric normal modes (a) of 90° twisted (Tw) hexatriene and its deuteriated forms.[a]

HT-d_0		3, 4-d_2-HT		2, 5-d_2-HT	
ν (cm^{-1})	γ	ν (cm^{-1})	γ	ν (cm^{-1})	γ
1497	0.00	1491	0.03	1488	0.04
1483	0.09	1472	0.06	1459	0.05
1317	0.12	1310	0.26	1275	0.06
1309	0.15	1248	0.02	1285	0.22
1192	0.00	1170	0.00	999	0.01
1136	0.00	886	0.01	1135	0.00
1035	0.00	1022	0.00	830	0.00
919	0.04	913	0.04	852	0.04
821	0.00	814	0.00	819	0.00
731	0.02	654	0.02	726	0.02
582	0.00	542	0.01	575	0.00
411	0.04	404	0.03	405	0.04
367	0.01	352	0.02	360	0.01
140	0.00	139	0.00	135	0.00
− 168	···	− 166	···	− 153	···

[a] Computed by QCFF/PI.

different pattern for the γ values and the Tw form shows a markedly different pattern from the other two forms.

For the deuteriated species the values of the γ's depend on the position of deuteriation. The high γ values for the modes above 1500 cm^{-1} persist for both the 3,4- and 2,5-deuteriated species in the E and Z forms. The largest γ's of the E form of 2,5-d_2-HT resemble those of E-hexatriene-d_0 whereas the γ's of E-3,4-d_2-HT are markedly changed. The Z form of 3,4-d_2-HT shows two large γ's for the modes at 1254 and 1294 cm^{-1} and that of 2,5-d_2-HT shows particularly one large γ at 1212 cm^{-1}. In the Tw geometry deuteriation at either 3,4- or 2,5-positions induces a pattern with essentially one large γ around 1300 cm^{-1}.

V. DISCUSSION OF RAMAN SPECTRA

A. Ground state

The ground state Raman and infrared spectra of the E and Z isomers of hexatriene-d_0 have been discussed in detail previously.[25] As the present calculations do not change that general picture this shall not be discussed further. The theoretical calculations on the 3,4- and 2,5-deuteriated species agree in general quite well with the experimental data. An exception is the b_g (EHT) or b_2 (ZHT) C=CH$_2$ twist mode computed in the region 585–615 cm^{-1}, which experimentally is found at much lower wave numbers.

B. Triplet state

We here discuss the experimental resonance Raman results of hexatriene-d_0 and the deuteriated hexatrienes in their triplet states in the light of the results from the theoretical calculations.

For heptatriene[32] and hexatriene[52] the triplet–triplet difference absorption spectrum extends experimentally from 350 to at least 300 nm with a first maximum in the region 300–315 nm. No experimental data below 300 nm are available. Calculations with QCFF/PI as well as CNDO/S Hamiltonians agree qualitatively in the prediction of a strongly allowed electronic $T_1 \rightarrow T_5$ transition for the planar E and Z geometries with a transition energy in the region 4.24–4.69 eV corresponding to 264–292 nm. In the 90° twisted geometry the lowest transition with an oscillator strength comparable to that of this strong transition is predicted around 5.49–5.75 eV, i.e., 216–226 nm. From these results it seems likely that the molecules responsible for the strong absorbance around 315 nm are in or close to the E or Z geometries. Furthermore, a much stronger resonance enhancement in Raman scattering must be expected from molecules being in the E and Z than in the twisted geometry when exciting with a wavelength around 315 nm. In fact, the distance in energy of the exciting laser frequency from the calculated Tw transition is about three times larger than from that of the E or Z transitions. This indicates that Raman intensity should be about an order of magnitude smaller for molecules in the Tw than for those in the E or Z geometries.

We have plotted the calculated values of the γ's for the E, Z and Tw forms of HT-d_0, 3,4-d_2-HT and 2,5-d_2-HT as stick diagrams as a function of wave number together with the experimentally obtained resonance Raman spectra in the T_1 state in Figs. 7–9. In the comparison of the stick diagrams the different $T_1 \rightarrow T_n$ transition energies for the E and Z forms compared to the Tw form should be kept in mind. Furthermore, any assignment of calculated vibrational bands to experimentally observed ones must be considered qualitative, when the computed γ values or the observed intensities are not large. We recall that besides the approximations mentioned above we have assumed no Duschinsky ef-

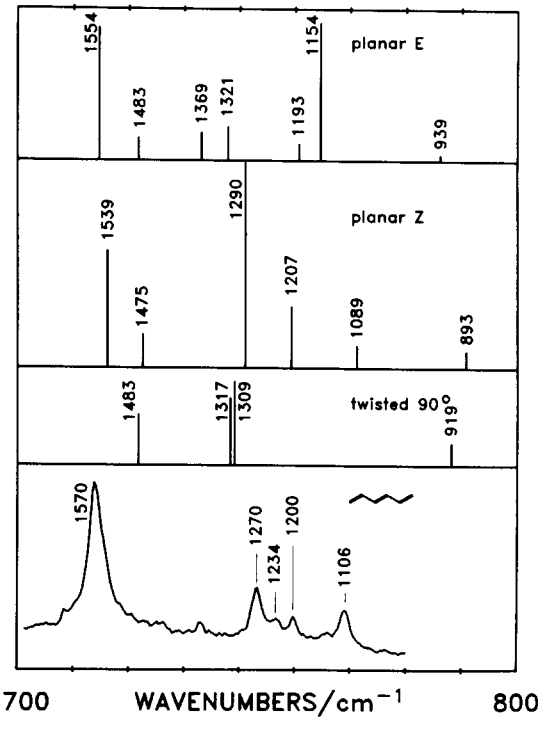

FIG. 7. Calculated wave numbers and relative γ-values for the totally symmetric vibrational modes of the E form in resonance with the $T_1 \rightarrow T_5$ transition, the Z form ($T_1 \rightarrow T_5$) and the Tw form ($T_1 \rightarrow T_6$) of 1,3,5-hexatriene-d_0 together with the experimental triplet state time-resolved resonance Raman spectrum.[35]

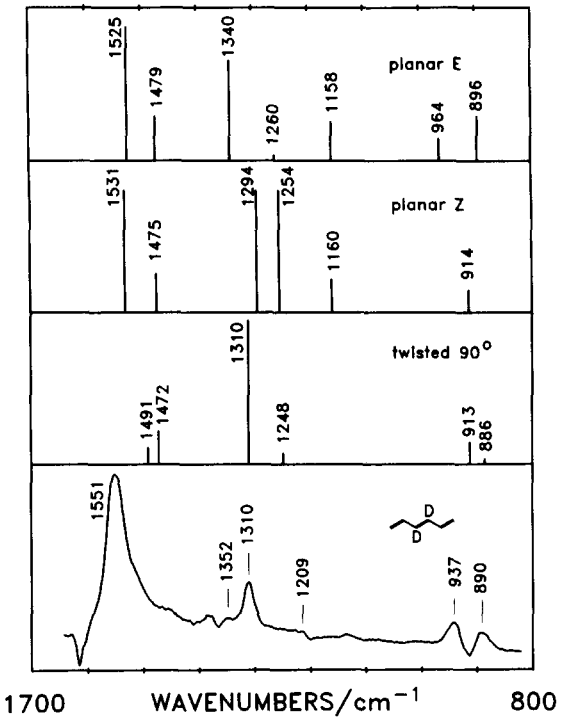

FIG. 8. Calculated wave numbers and relative γ-values for the totally symmetric vibrational modes of the E form in resonance with the $T_1 \rightarrow T_5$ transition, the Z form ($T_1 \rightarrow T_5$) and the Tw form ($T_1 \rightarrow T_6$) of 3,4-d_2-1,3,5-hexatriene together with the experimental triplet state time-resolved resonance Raman spectrum [see Fig. 4(A)].

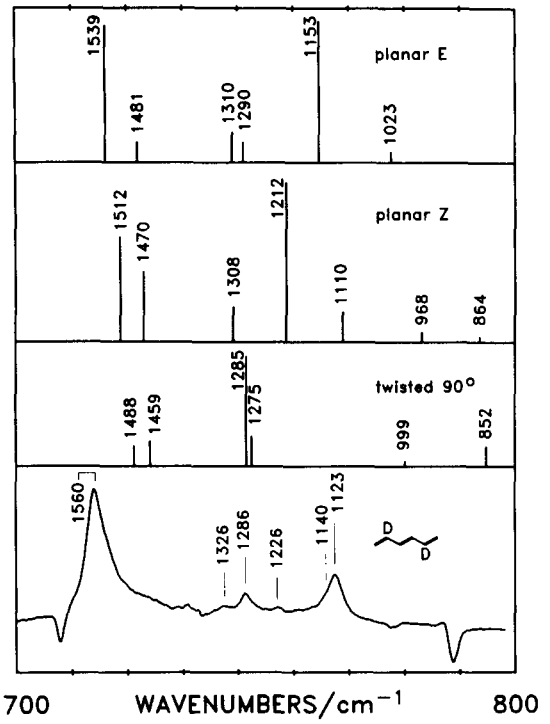

FIG. 9. Calculated wave numbers and relative γ-values for the totally symmetric vibrational modes of the E form in resonance with the $T_1 \rightarrow T_5$ transition, the Z form ($T_1 \rightarrow T_5$), and the Tw form ($T_1 \rightarrow T_6$) of 2,5-d_2-1,3,5-hexatriene together with the experimental triplet state time-resolved resonance Raman spectrum [see Fig. 4 (C)].

fect between T_1 and T_n. We have checked that such an effect is not very important in planar forms since diagonal terms of the rotation matrix are $\geqslant 0.90$. We first discuss hexatriene-d_0.

From the appearance of strong Raman bands above 1500 cm^{-1} we must conclude that a considerable part of the hexatriene molecules is in the E or Z geometry or in both. The Tw form cannot account for any band with strong intensity above 1500 cm^{-1}. From the appearance of the experimental spectrum we feel confident to assign the experimental band at 1106 cm^{-1} to the calculated band of the E form at 1154 cm^{-1} and the experimental band at 1270 cm^{-1} to that of the Z form at 1290 cm^{-1} and finally the strong experimental band at 1570 cm^{-1} to a superposition of calculated bands from the E form at 1554 and the Z form at 1539 cm^{-1}. Finally the experimental band at 1200 cm^{-1} is tentatively assigned to the Z form at 1207 cm^{-1}. Thus the resonance Raman spectrum can be explained as a superposition of the spectra of the E and Z forms without any contribution of the Tw form. It follows that the E and Z forms are present in T_1 with comparable weight. Although no indication of the Tw form is found in the resonance Raman spectrum, caution should be exerted in ruling out its presence, considering its less favorable resonance conditions, compared to the other two forms, under the present experimental conditions.

Turning now to the deuteriated species, the experimental band of E-3,4-d_2-HT at 1551 cm^{-1} can be assigned to either the E or the Z form. It should be noted that the calculations correctly predict a lower wave number of this band for the 3,4-deuteriated species than for EHT-d_0. The other rather strong experimental band at 1310 cm^{-1} can be assigned to either a calculated band of the E form at 1340 cm^{-1} or one of the two bands of the Z form at 1254 and 1294 cm^{-1}. Furthermore, a weak contribution from the mode calculated at 1310 cm^{-1} from the twisted form to this band cannot be ruled out completely. The experimental bands at 937 and 890 cm^{-1} can be assigned either to the two bands of the E form at 964 and 896 cm^{-1} or to the band of the Z form at 914 cm^{-1}. Finally the weak experimental bands at 1209 and 1352 cm^{-1} can probably be explained by some of the weaker calculated bands. Hence the experimental resonance Raman spectrum of E-3,4-d_2-HT indicates clearly the presence of the E form but does not allow firm conclusions on that of the Z form. Again the presence of the Tw form cannot be excluded from the present experiments. The experimentally found triplet state resonance Raman spectrum of E-2,5-d_2-HT leads to similar conclusions. Again the strong band at 1560 cm^{-1} can be assigned to the E form (1539 cm^{-1}) and/or the Z form (1512 cm^{-1}). The other strong band at 1123 cm^{-1} has a shoulder at $\sim$1140 cm^{-1}. We assign the 1123 cm^{-1} band to the calculated band of the E form at 1153 cm^{-1} and the shoulder to the 1212 cm^{-1} band of the Z form. The weaker experimental band at 1286 cm^{-1} can then either be assigned to calculated bands at 1290 or 1310 cm^{-1} of the E form or to the band at 1308 cm^{-1} of the Z form. Again, a contribution from the band calculated at 1285 cm^{-1} from the twisted form cannot be ruled out definitively. Hence the presence of the E form of E-2,5-d_2-HT is clearly indicated,

whereas that of the Z form seems likely in smaller concentration.

In conclusion, the calculated wave numbers of the totally symmetric normal modes in the T_1 state and the calculated γ values for the $T_1 \rightarrow T_n$ transitions from the planar E and Z forms of hexatriene-d_0 and dideuteriated hexatrienes provide a good basis for the understanding of the triplet state resonance Raman spectra. A comparison between the calculated and experimentally found resonance Raman spectra of EHT-d_0, E-3,4-d_2-HT, and E-2,5d_2-HT in their triplet state T_1 clearly indicates that the predominant form in the triplet state of these molecules probed by the present resonance Raman experiments is the planar E form. The presence of the Z form is indicated as well, particularly by the spectra of EHT-d_0, which cannot be explained by the E form only. The twisted Tw form may be present, but its Raman spectrum is expected to be weaker by about an order of magnitude under the present experimental conditions.

VI. CONCLUSION

We have recorded the time-resolved resonance Raman spectra of E-3,4-d_2-hexatriene and E-2,5-d_2-hexatriene in their lowest T_1 states. These spectra together with the spectrum of E-hexatriene-d_0 obtained previously[35] are compared with results from theoretical calculations, based on QCFF/PI and CNDO/S Hamiltonians, in an attempt to determine the stable structures of these flexible molecules. To this end equilibrium geometries and minimum energies are computed for the planar E and Z forms in the S_0 and T_1 states and for the Tw form in the T_1 state. The relative energies of Tw and Z optimized geometries are found to be 7.1 and 1.1 kcal/mol, respectively, taking the energy of the E geometry as reference.

To allow interpretation of resonance Raman spectra, energies of higher triplet states up to T_8 are calculated for the three geometries together with oscillator strengths for the $T_1 \rightarrow T_n$ transitions. Only one strong transition is found up to 6 eV above T_1 for each of the three forms (E, Z and Tw). For the E and Z forms this transition is the $T_1 \rightarrow T_5$ transition at about 4.3 eV, while for the Tw form the $T_1 \rightarrow T_6$ transition at about 5.5 eV is by far the strongest. A comparison of the computed energy gaps with the maximum in the $T_1 \rightarrow T_n$ difference absorption spectrum, located around 300 nm,[52] indicates that both planar forms (E and Z) are populated in the T_1 state.

The resonance Raman intensities of a_g vibrational modes in T_1 can then be estimated under the assumption of a dominant Franck–Condon mechanism for each of the three forms E, Z, and Tw and for HT-d_0, 3,4-d_2-HT and 2,5-d_2-HT. The observed resonance Raman spectra can be satisfactorily attributed to the E and Z forms. This result, which modifies a previous suggestion,[35] confirms that in T_1 the E and Z forms are substantially populated. While there is no direct evidence for Tw population in T_1, the weakness of the $T_1 \rightarrow T_n$ transition near 4.3 eV for this form, compared to the E and Z forms, cautions against the conclusion that this population is negligible.

ACKNOWLEDGMENTS

This work was supported by a collaborative research grant (Grant No. 0137/88) from NATO, by the Danish Natural Science Research Council, and by the Ministero della Pubblica Istruzione of Italy. The authors thank Dr. H. J. C. Jacobs, Professor W. Siebrand and Dr. A. A. Gorman for helpful discussions and Dr. K. B. Hansen for continual support with the experimental facility. Also the help of H. Egsgaard with the GC apparatus, Dr. O. F. Nielsen with the Raman spectrometer and Dr. J. Fenger and P. Genske with the lasers is gratefully acknowledged.

[1] B. S. Hudson, B. E. Kohler, and K. Schulten, in *Excited States*, edited by E. C. Lim (Academic, New York, 1982), Vol. 6, pp. 1–95.
[2] R. J. Hemley, A. C. Lasaga, V. Vaida, and M. Karplus, J. Phys. Chem. **92**, 945 (1988).
[3] V. Bonačić-Koutecky and S. Ishimaru, J. Am. Chem. Soc. **99**, 8134 (1977).
[4] M. Said, D. Maynau, and J.-P. Malrieu, J. Am. Chem. Soc. **106**, 580 (1984).
[5] M. A. C. Nascimento and W. A. Goddard III, Chem. Phys. Lett. **60**, 197 (1979).
[6] M. A. C. Nascimento and W. A. Goddard III, Chem. Phys. **36**, 147 (1979).
[7] C. W. Bock, Y. N. Panchenko, S. V. Krasnoshchiokov, and V. I. Pupyshev, J. Mol. Struct. (Theochem) **148**, 131 (1986).
[8] B. A. Hess, Jr. and L. J. Schaad, J. Am. Chem. Soc. **105**, 7500 (1983).
[9] G. Fogarazi, P. Szalay, P. P. Liescheski, J. E. Boggs, and P. Pulay, J. Mol. Struct. **151**, 341 (1987).
[10] P. G. Szalay, A. Karpfen, and H. Lischka, J. Chem. Phys. **87**, 3530 (1987).
[11] C. W. Bock, P. George, and M. Trachtman, J. Mol. Struct. (Theochem) **109**, 1 (1984).
[12] I. Ohmine and K. Morokuma, J. Chem. Phys. **73**, 1907 (1980).
[13] (a) A. Warshel and M. Karplus, Chem. Phys. Lett. **17**, 7 (1972); (b) A. Warshel and P. Dauber, J. Chem. Phys. **66**, 5477 (1977).
[14] (a) A. C. Lasaga, R. J. Aerni, and M. Karplus, J. Chem. Phys. **73**, 5230 (1980); (b) R. J. Hemley, B. R. Brooks, and M. Karplus, J. Chem. Phys. **85**, 6550 (1986).
[15] M. Traetteberg, Acta Chem. Scand. **22**, 628 (1968).
[16] M. Traetteberg, Acta Chem. Scand. **22**, 2294 (1968).
[17] L. R. Lippencott, C. E. White, and J. P. Sibilia, J. Am. Chem. Soc. **80**, 2926 (1958).
[18] L. R. Lippencott and T. E. Kenney, J. Am. Chem. Soc. **84**, 3641 (1962).
[19] Yu. N. Panchenko, Yu. A. Pentin, and E. B. Rusach, Russ. J. Phys. Chem. **49**, 1536 (1975).
[20] Yu. N. Panchenko, P. Császár, and F. Török, Acta Chim. Hung. **113**, 149 (1983).
[21] Yu. N. Panchenko and E. B. Rusach, Moscow Univ. Chem. Bull. **20**, 221 (1979).
[22] D. Raković, S. A. Stepanyan, L. A. Gribov, and Yu. N. Panchenko, J. Mol. Struct. **90**, 363 (1982).
[23] B. U. Curry, Ph.D. thesis, University of California, Berkeley, 1983.
[24] R. McDiarmid and A. Sabjić, J. Phys. Chem. **91**, 276 (1986).
[25] F. W. Langkilde, R. Wilbrandt, O. F. Nielsen, D. H. Christensen, and F. M. Nicolaisen, Spectrochim. Acta Part A **43**, 1209 (1987).
[26] Y. Furukawa, H. Takeuchi, I. Harada, and M. Tasumi, J. Mol. Struct. **100**, 341 (1983).
[27] M. Tasumi and M. Nakata, J. Mol. Struct. **126**, 111 (1985).
[28] D. F. Evans, J. Chem. Soc. **1960**, 1735.
[29] N. G. Minnaard and E. Havinga, Recl. Trav. Chim. **92**, 1179 (1973).
[30] R. McDiarmid, A. Sabljić, and J. P. Doering, J. Am. Chem. Soc. **107**, 826 (1985).
[31] A. A. Gorman, I. Hamblett, M. Irvine, P. Raby, M. C. Standen, and S. Yeates, J. Am. Chem. Soc. **107**, 4404 (1985).
[32] F. W. Langkilde, R. Wilbrandt, and N.-H. Jensen, Chem. Phys. Lett. **111**, 372 (1984).
[33] F. W. Langkilde, N.-H. Jensen, and R. Wilbrandt, Chem. Phys. Lett. **118**, 486 (1985).
[34] F. W. Langkilde, N.-H. Jensen, R. Wilbrandt, A. M. Brouwer, and H. J. C. Jacobs, J. Phys. Chem. **91**, 1029 (1987).

[35]F. W. Langkilde, N.-H. Jensen, and R. Wilbrandt, J. Phys. Chem. **91**, 1040 (1987).
[36]J. Levisalles, Bull. Soc. Chim. France **1957**, 997.
[37]A. M. Brouwer, J. Cornelisse, and H. J. C. Jacobs, J. Photochem. Photobiol. A **42**, 313 (1988).
[38]A. B. Myers, R. A. Mathies, D. J. Tannor, and E. J. Heller, J. Chem. Phys. **77**, 3857 (1982).
[39]A. Warshel and M. Karplus, J. Am. Chem. Soc. **94**, 5612 (1972).
[40]A. Warshel and M. Levitt, QCPE No. 247, Indiana University 1974.
[41]A. Warshel, in *Modern Theoretical Chemistry*, edited by A. Segal (Plenum, New York, 1977), Vol. 7, Part A p. 133.
[42]B. Hudson and J. Andrews, Chem. Phys. Lett. **63**, 493 (1979).
[43]G. Orlandi and F. Zerbetto, Chem. Phys. **123**, 175 (1988).
[44]D. R. Armstrong, R. Fortune, P. G. Perkins, and J. J. P. Stewart, J. Chem. Soc. Faraday Trans. 2 **68**, 1839 (1972).
[45]F. Zerbetto, Dissertazione di Dottorato di Ricerca, Bologna, 1986.
[46]C. A. Coulson and H. C. Longuett-Higgins, Proc. R. Soc. London Ser. A **191**, 39 (1947).
[47]F. Negri, G. Orlandi, F. Zerbetto, and M. Zgierski (unpublished results).
[48]H. C. Longuett-Higgins and J. A. Pople, Proc. Phys. Soc. London Sect. A **68**, 591 (1955).
[49]J. Del Bene and H. H. Jaffe, J. Chem. Phys. **48**, 1807 (1968).
[50]G. Maier, H. P. Reisenauer, B. Rohde, and K. Dehnicke, Chem. Ber. **116**, 732 (1983).
[51]F. Duschinsky, Acta Physicochim. USSR **7**, 551 (1937).
[52]A. A. Gorman (private communication).